



This is to certify that the

thesis entitled

# SCALING EFFECT OF MECHANICAL FASTENING ON COMPOSITE STRUCTURES

presented by

JUNLING YOU

has been accepted towards fulfillment of the requirements for

\_\_\_\_degree in \_\_\_\_\_

M.S.

Major professor

Date 5/8/98

O-7639

MSU is an Affirmative Action/Equal Opportunity Institution

LIBRARY
Michigan State
University

PLACE IN RETURN BOX to remove this checkout from your record.

TO AVOID FINES return on or before date due.

DATE DUE	DATE DUE	DATE DUE
**************************************		

1/98 c/CIRC/DateDue.p65-p.14

# SCALING EFFECT OF MECHANICAL FASTENING ON THICK COMPOSITE STRUCTURES

By

Junling You

#### A THESIS

Submitted to
Michigan State University
in partial fulfillment of the requirements
for the degree of

MASTER OF SCIENCE

Department of Materials Science and Mechanics

1998

#### **ABSTRACT**

# SCALING EFFECT OF MECHANICAL FASTENING ON THICK COMPOSITE STRUCTURES

By

#### Junling You

Mechanical joints are suitable for joining composite laminates, especially thick-section composites. In most studies on mechanical joints, the interactions between pin diameter (D) and composite dimensions such as width (W) and distance from hole center to composite end (e), i.e. W/D and e/D ratios, were the primary concerns. However, as composite thickness increases, the contact interaction between the pin and composite becomes more complicated. This study investigated the mechanical joint efficiency of a composite material made of woven glass fabric and phenolic matrix. Sixteen joint configurations based on four composite thicknesses and four pin diameters were examined. Both experimental method and finite element analysis were performed in this study. Results showed that thick composites with small pins and thin composites with large pins had lower efficiencies of joint stiffness and joint strength than those having similar dimensions between pin diameter and composite thickness.

## ACKNOWLEDGEMENTS

The author wishes to express her sincere thanks to Professor Dahsin Liu in the Department of Materials Science and Mechanics, and also thanks to U. S. Army - TARDEC for financial support.

### **TABLE OF CONTENTS**

LIST OF TABLES	vi
LIST OF FIGURES	vii
CHAPTER 1	
INTRODUCTION	1
Literature Review	1
Statement of the Problem and Objective	11
Organization of Thesis	12
CHAPTER 2	
EXPERIMENTAL METHOD	14
Composite Material	14
Composite Thickness	14
Pin Diameter	16
NTRODUCTION  Literature Review  Statement of the Problem and Objective  Organization of Thesis  HAPTER 2  XPERIMENTAL METHOD  Composite Material  Composite Thickness  Pin Diameter  Composite Mechanical Joint  Experimental Results  HAPTER 3  OMPUTATIONAL METHOD  Finite Element Method  Finite Element Model  Finite Element Analysis  Computational Results  HAPTER 4  ONCLUSIONS AND RECOMMENDATIONS  Conclusions  Recommendations	26
CHAPTER 3	
COMPUTATIONAL METHOD	36
Finite Element Method	36
Finite Element Model	38
Finite Element Analysis	53
CHAPTER 4	
CONCLUSIONS AND RECOMMENDATIONS	87
REFFERENCES	91

## LIST OF TABLES

Table 1: Linear orthotropic material properties determined from experiments and assumed (underlined) for computer simulations
Table 2: Ratios of $\frac{W}{D}$ , $\frac{e}{D}$ , and $\left(\frac{H}{D}\right)^2$
Table 3: Specimen nomenclature for various combinations of pin diameter and plate thickness
Table 4: Experimental results of joint stiffness and joint stiffness per unit bearing area . 22
Table 5: Experimental results of the type of load-deformation relation, joint strength, and offset deformation percentage from linear range
Table 6: Numbers of elements used around the hole edge
Table 7: Numbers of layers used in the thickness directions
Table 8: Loading used in finite element linear analysis
Table 9: Bending behavior of the pin after deformation from linear analysis 60
Table 10: Computed results of the node numbers and locations in polar coordinates for the maximum bearing stresses
Table 11: Joint stiffnesses from both experiments and computations
Table 12: Joint strengths from both experiments and computations
Table 13: Joint strengths from experiments and nonlinear computations
Table 14: Joint stiffnesses from experiments and nonlinear computations

# LIST OF FIGURES

Figure 1 - Schematic diagram for double-lap, single-pin joint
Figure 2 - Progressive hole drilling in composite joint system
Figure 3 - Load-deformation relation for D2H2, a type A joint
Figure 4 - Load-deformation relation for D4H4, a type B joint
Figure 5 - Load-deformation relation for D8H8, a type C joint
Figure 6 -Pin subjected to bearing forces
Figure 7Schematic diagram for double-lap, single-pin joint in computational method . 39
Figure 8 -Symmetric boundary conditions for computer simulation model 41
Figure 9 - The finite element mesh of joint D1H1
Figure 10 -The finite element mesh around the contact area of joint D1H1 46
Figure 11 -Nonlinear stress-strain relation of composite material
Figure 12 -Nonlinear analysis computer simulation process
Figure 13 -Bending behavior of the pin in joint D8H1
Figure 14 -The contact normal stresses on the pin contact surface for joint D1H1 64
Figure 15 -The contact shear 1 stresses on the pin contact surface for joint D1H1 65
Figure 16 -The contact shear 2 stresses on the pin contact surface for joint D1H1 66
Figure 17 -The in-plane tensile stresses of the central composite plate for joint D1H1 69
Figure 18 -The in-plane shear stresses of the central composite plate for joint D1H1 70
Figure 19 -The in-plane compressive stresses of the central composite plate for joint D1H1
Figure 20 -Comparison of joint stiffnesses
Figure 21 -Comparison of joint strengths

Figure 22 -Load-deformation relation of joint D1H1 from computational results	79
Figure 23 -Comparison of joint strengths	82
Figure 24 -Extended damage of D8H1 joint	83
Figure 25 -Comparison of joint stiffnesses	86

#### CHAPTER 1 INTRODUCTION

#### 1. Literature Review

Composite materials are commonly used in recent years in structures which demand a high level of mechanical performance. The success of composite materials in replacing conventional metals is primarily due to their high specific strengths and stiffnesses coupled with cost effectiveness. Improvements in understanding of the mechanics of composite materials, and advances in the technology of making and using them, are greatly extending the range of potential applications of these materials. Examples of the use of composite materials which can be found in the automotive, aerospace and defense industries were once reported by Harris and Morris [1]. However, studies of composite materials have tended to be limited to thin shell structures such as aircraft fuselages or pressure vessels due to the ease in making and designing them.

As the technologies of composite manufacturing advance and the applications of composites to non-aerospace industries are identified, more and more thick-section composites are used for structure applications. For example, thick-section composites used for the submarine hull and armor vehicle bodies have been proved to be feasible. It is believed that thick-section composites have many advantages that thin-section composites cannot provide. Bogetti and Gillespie [2] reported the growing interest in thick-section composites.

The extension from thin plates applications to thick-section composites applications, however, is not trivial. In fact, it requires careful modifications in almost every aspect of

composite technologies, e.g., manufacturing, testing, analysis, and design. Taking composite joining as an example, the design of an adhesive joint may turn out to be impractical if the composite become very thick. Since thick-section composites behave differently from their thin-section counterparts, investigations on thick composites should be performed carefully [3]. Increasing application of thick-section composites has prompted increasing research activities, both analytical and experimental.

Investigations on thick composites can be found in the literature. Twardowski [4] obtained thick part (>5 cm) temperature profiles from a one dimensional experiment, and compared the experimental results with the predictions of a computer simulation containing improved and existing models for extent of reaction, viscosity and other composite properties of the same resin/fiber system. The following results were found: the initial extent of reaction was relatively unimportant; the viscosity never reached low values simultaneously through the thickness in laminates which were in excess of 10 cm thickness. Based on strain energy approaches and finite element techniques, an effective property model was developed by Alexander and Tzeng [5] to compute the properties for an arbitrarily shaped element with multiple anisotropic material regions. The effective material stiffness calculated by the model was compared to those by other models, results showed that this model was especially suitable for thick composites. An analytical model for the buckling of thick wall orthotropic composite pipe under external pressure has been developed by Yang et al [6]. First-order laminated anisotropic plate theory was used to construct models of the kinematic and constitutive behavior of the composite cylinders. The Ritz Method was then applied to determine the buckling load under external pressure. Results obtained from the developed model were compared with the theory derived by Flugge and experimental results, good agreement was found. Avva et al [7] measured the through-the-thickness strength of three-dimensional triaxially braided graphite/epoxy composites and compared it with an equal thickness and fiber orientation laminated graphite/epoxy composite. Laminated specimens were made from AS4/3501-6 graphite/epoxy prepreg using hand lay-up molding and autoclave curing and tested in a uniaxial tension machine. A simple curved beam equation was used to calculate the through-the-thickness strength of composites from the measured failure load. Results showed that the strengths of braided and equivalent laminated composites were nearly equal within the data scatter. Through-the -thickness strength of both braided and laminated composites was found to be a matrix dependent property.

Studies of thick composites focused on failure analysis were also performed by some researchers. Nguyen [8] extended the Renard et al's [9] transverse matrix cracking model to the three-dimensional analysis of laminated composite structures. The generalized model was implemented in the general finite element system. It was based on the continuum damage mechnics and used with the composite three-dimensional multilayer finite elements to determine the development of transverse matrix cracking in complex composite structures under quasi-static loadings where the three-dimensional stress state has to be considered. The results from the presented approach were compared with the classical approaches of damage, which generally use phenomenological failure criteria to predict the strength of composites and impose arbitrarily small components of the stiffness matrix when the failure occurs. The former was more precise since the last on describes more realistically the behavior of composites until their ultimate failure. Camponeschi et al [10] described an analysis of 6.4-25.4 mm thick composite laminates subjected to uniaxial

compressive loading that experimentally showed a decrease in strength with increasing thickness. The analysis was based on closed form solutions for the formation of kink-band failures in the presence of fibers misaligned with the principal axis of compression loading. The fiber misalignment was determined by a finite element analysis that accounted for the displacement of the laminated outer plied where the laminate exited the compression test fixture. The correlation between the experimental results and the theoretical analysis showed that the compression strength of the AS4/3501-6 and S2/3501-6 laminates to be independent of the thickness and directly proportional to the through-the-thickness fixture restraint on the through-the-thickness Poisson expansion. A practical computational procedure based on global/local finite element method was developed by Woo and Whitcomb [11] for detailed failure analysis of thick textile composites. The procedure utilizes two problem levels: global and local levels. An initial global solution was obtained using a coarse global mesh, and a small portion of the textile composite was modeled with a refined local mesh. Infinitely repeating plain weave unit cell and finite thickness plain weave configurations under tension load were considered to study the stress and failure behavior. Results indicated that the failure behavior of plain weave textile composites was sensitive to the fiber bundle waviness. The initial failure mode was the fiber bundle separation when the waviness ratio was large while it was the fiber bundle fracture when the waviness ratio was small. It was also found that the stress distributions near the free surface were different from those inside. The stress level was much higher inside than near the free surface while the boundary region was shallow and was limited to the outer-most layer.

Composite joining is a study of assembling technique in composite structural

components together. Both mechanical fastening and adhesive bonding are commonly used in composite joining. In mechanical fastening, a pin is inserted through holes of several composite laps. The composite laps are usually thin shells. As the applications of the composite structure expand, more and more thick composite sections are used in industries. However, the change from two-dimensional thin shells to three-dimensional thick sections can greatly alter the contact mechanisms between the fastener and the composite. Subsequently the stress distributions in thick composites will be different from those expected on the bases of conventional thin composite designs. Certainly, the failure mechanism may change, and unexpected failures or expensive over-design might result. That is to say, unwise extension of thin-wall design procedures to thick sections can cause the design process to lose its major significant assets, those can be predictable and controled. On the contrary, adhesive bonding is impractical if composite thicknesses become very large. Hence, mechanical fastening has been an important assembling technique for joining composite structures.

Many articles regarding the study of mechanical fastening for thin-shell composite structures can be found in the literature. For example, Hamada et al [12] presented a study on predicting the joint strength of mechanical fasteners. Two joint geometries that exhibit net-section failure and bearing failure were chosen to examine the prediction method in consideration with bearing failure. The idea of combining the Yamada-Sun failure criterion and the characteristic length appears in the formulation of the point stress criterion reported by Whitney and Nuismer [13] was used in the prediction method, the definition method of the characteristic length for compression was most important for predicting the bearing strength. Good agreement was found between the experimental and predicted

results. Dattaguru and Rao [14] studied the contact problems of fastener joints in composite plates, the contact constraint methods, friction laws, contact searching algorithms and possible solution techniques were presented de Jong [15] dealt with stresses in infinite plates, the loading force being in equilibrium with infinitely small, uniformly distributed forces at infinity. A solution was presented for the stress distribution around an unreinforced hole in an orthotropic plate, loaded on only a part of its edge by an infinitely rigid pin of material, there was assumed to be no friction. It was concluded that in the pinloaded infinite plate there was a clearance, resulting from elastic deformations of the plate material, not only between the pin and the lower half of the hole, but also between the pin and a small part of the upper half. Waszcac & Cruse [16] studied the stresses in infinite plates, the loading force being in equilibrium with infinitely small, uniformly distributed forces at infinity. The solutions are applicable to joints with large interferes between the pin and the hole. de Jong [17] investigated the stress distribution around a pin-loaded hole in an elastically isotropic or orthotropic plates. The hole was loaded frictionless on only a part of its edge by an infinitely rigid pin of the same diameter. The loading force was carried over on the edge by normal stresses, represented by a sine series. The numerical results showed that the stress distribution depended strongly on the material properties. Lessard et al [18] studied the modeling of damage in a laminated composite pinned-joint using finite element method. A laminated composite plate with a circular hole filled with a rigid pin where the load was applied at one end of the plate and this load was resisted by the rigid pin. Results indicated that two-dimensional linear and non-linear modeling could predict final failure load, and three-dimensional modeling methods could be extended from these two-dimensional methods required further work.

It is well known [19, 20] that fasteners can severely reduce the load-carrying capability of the components by more than fifty percent. Due to anisotropy and inhomogeneity of composites, the failure and strength of bolted composite joins can be considerably different from the failure and strength of metallic joints. Damage in bolted composite joins can initiate at an early loading stage and accumulate inside the laminates as the load increases. The accumulation of damage and the mode of failure strongly depend upon the material. ply orientation, laminate thickness, joint geometry, and loading condition, etc. As a consequence, the strength and failure of bolted composite joints are significantly influenced by the damage accumulated inside the composites. Hence, failure analysis is very important in composite joints studies. Wang et al [21, 22] performed an investigation to study the bearing failure and response of a mechanically fastened laminated composite joint. The results of the study were presented in two parts: experimental characterization and analytical prediction. Only double-lap metal/composite/metal bolted joints were considered. In experiments, a load cell was designed and manufactured which was mounted on the fastener to monitor the bolt clamping pressure as a function of the applied load. An accumulative damage model based on the damage mechanisms observed from the experimental study was developed to simulate the bearing failure in the laminated composite joints. The prediction was in good agreement with the data. Based on the experimental results, it could be concluded that the lateral support was crucial for bolted laminated composite joints. Bearing damage could be catastrophic if there was no lateral support. Shear cracks induced by accumulated compression failure appeared to be the primary failure mode of the bearing damage. Lateral supports could suppress the shear crack propagation and change failure from a catastrophic to a progressive failure mode. Clamping pressure could

increase bearing strength. It was believed that the model could be extended to three dimensions in order to simulate accurately the bearing response of bolted composite joints in real structures.

Mechanical joints for thin composites are usually investigated in laboratories for joint characterizations. Results from the thin composite joints studies are then used for thick composite joint designs. However, thin composite joints do not always behave the same as the thick composite joints made of identical material, that is to say, if mechanical joints are to be used in composite assembly, the differences between two-dimensional thin shells and three-dimensional thick sections will greatly alter the contact mechanisms between the pins and the composites; subsequently the stress distributions in the thick-section composites will be different from those in the thin shells, so will be the failure mechanisms.

There has been some achievements regarding the study of stress analysis of mechanical fastening for thick-section composite structures. Sperling [23] computed the three-dimensional stress distribution around pin-loaded holes in composite laminates using finite element method. A rigid pin and an elastic bolt were both considered. The results showed that stresses around the pin-loaded holes varied not only with the angles along the hole surface, but did also vary through the laminate thickness. By replacing the rigid pin by an elastic bolt it was found that the stress distribution around the hole changed significantly and depended on the bolt stiffness. Sundarrai and Dataguru [24] presented a study of stress distribution in a double-shear lap joint with an interference-fit pin subjected to inplane loading by using three-dimension finite element analysis. The results graphically showed the through-the-thickness stress distribution and the beneficial effects of interference on fatigue life of the joint. Hwang and Stallings [25] reported a two-dimensional

unsymmetrical finite element model and a three-dimensional solid finite element model generated to investigate the stress behaviors in high pressure bolted flange joint. Comparisons between the experimental results and the computer simulation results from these two models showed the feasibility of these models. Griffin et al [26] gave a numerical procedure for determining loading proportioning in composite joints. The joints in this paper were of single pin, double lap fashion and loaded in tension. The commercial finite element program ABAQUS was used to predict the loading proportioning among fasteners through two plane-stress finite element models, one model represented for the composite inner lap and the other for the two steel outer laps. The results indicated the accuracy of this numerical procedure. Ireman et al [27] discussed problems related to the determination of the load distribution in a multi-fastener joint using the finite element method, such as the stress singularities at the interface. Results showed that the mesh refinement must be applied to obtain more accurate results. Madenci and Ileri [28] focused on the assessment of the contact stresses in mechanical joints with single fastener, with two fasteners, and with a row of fasteners perpendicular to loading in finite composite laminates. The solution was obtained by solving the governing equations of elasticity under plane-stress assumptions and modified mapping-collocation method. The load exerted by the fastener through the contact region, which consists of no-slip and slip zones due to the presence of friction, was modeled with appropriate mixed boundary conditions. The importance of the study of the contact stresses in mechanical joints was indicated through the results.

Since test specimens and computing cost is an important factor, two-dimensional finite element techniques has been used to analyze the pin-loaded case. However, by considering out-of-plane behavior of pin-loaded cases, such as edge effects, delamination, etc., the

failure behavior of composite plates becomes a three-dimensional problem, and the two-dimensional assumption may not be accurate or sufficient. Therefore, three-dimensional studies is unavoidable for failure analysis of mechanical fastening. Shokrieh and Lessard [29] established a three-dimensional nonlinear finite element code to analyze the effects of material nonlinearity on the state of stress and failure prediction near the stress concentrations of a pin-loaded laminated composite plate. A composite plate with a pin-loaded hole was considered, the pin was fixed and the load was applied on the other end of the composite plate. The results of prediction of failure initiation load by considering the material nonlinearity was in excellent agreement with experimental results. The results obtained from failure analysis emphasize that considering the material nonlinearity, especially for highly shear induced cases like [+454/-454]s was important in failure analysis of composite laminates using stress based failure criteria.

Small coupons are usually used in laboratories for material characterizations. Results from small coupon tests are then used for large structural designs. However, small coupons do not always behave the same as the large structures made of identical materials. The difference of behaviors due to size difference is usually called scaling effects. Scaling effects include both in-plane scaling effect and thickness scaling effect. The former has gained more attention than the latter possibly due to the fact that most conventional composite material are thin plates. Some investigations on the performance of composite materials and structures at different sizes have been presented by Rajapakse [30]. It has been concluded that scaling effects should be carefully examined in material characterizations and structural designs.

Scaling effects in two-dimensional problems, that is, in-plane scaling effect, has been

discussed by some researchers. The interactions between pin diameter (D) and composite dimensions such as width (W) and distance from hole center to composite end (e), i.e. W/D and e/D ratios, were of the primary concerns. Waszcac and Cruse [16] reported that the stress distribution around the pin-loaded hole depends on the ratios of width of plate to hole diameter. The results from Sperling [23], Marshall et al [31], Hamada et al [32], and Lassard [29] gave the relation between the ratios of the plate width to the pin diameter (W/D) and the net-section failure, the relations between the ratio of the distance to plate end to the pin diameter (e/D) and the shear-out failure. In order to avoid the net-section failure and the shear-out failure taking place before bearing failure, the W/D and e/D ratios should be at least 4 or greater.

To the best knowledge of the author, no literature has ever discussed the scaling effect in the thickness direction, that is, thickness scaling effect. The design of mechanical fastening for composites has tended to be done on a case-by-case basis. Studies of mechanical fastenings for composites with various thicknesses would be very tedious if no "unified rule" is included or developed. Alternatively, the study may be very efficient if some fundamental knowledge for thin composite mechanical fastening can be "transformed into" that for thick composite mechanical fastening. In other words, it will prove to be very useful if fundamentals of thickness scaling effects can be extracted from the existing information for thin composite fastening and some extra, but limited, studies on thick composite fastening.

#### 2. Statement of the Problem and Objective

There are obvious advantages, in utilizing very thick composites for bodies and hulls of combat vehicles. The joining of these components to substructure or other components must be, to a large degree, by mechanical fastening in order to gain high load-carrying capability and ease of structural disassembly. In the analysis of composite joints, contact mechanisms between the pins and the composites are strongly affected by the thickness of the composites. The contact condition along the pin is not uniform. Accordingly, three-dimensional composite joints need to be studied. In other words, the study to identify the interaction between the pin diameter and the composite thickness becomes the primary concern in composite joint analysis. Since both pin diameter and composite thickness are subjected to change, different combinations will result in different stress distributions, and subsequently strengths. In fact, there exist scaling effects in composite joint analysis.

Although the mechanical test can give both the stiffnesses and the strengths of the composite joints, it cannot give the detail stress information in the structure. Besides, it is very costly to perform a great amount of experiments. Hence, numerical analysis becomes very important since it is more efficient. Various scales composite joint can be examined from computer simulations. Accordingly, in this study, the objective is to investigate the composite joints with various thicknesses and pin sizes.

#### 3. Organization of Thesis

Four chapters were given in the thesis. Chapter 1, Introduction, includes the literature review, the statement of the problem, the objective of the study, and the organization of the thesis. Chapter 2, Experiment Method, briefly reports the testing methods involved in

the investigation. Chapter 3, Computational Method, gives the general idea of the important role of the computer simulation in this study and the techniques of the numerical method. Chapter 4, Conclusions and Recommendations, summarizes the finding from the investigations and gives suggestions for future work.

#### **CHAPTER 2 EXPERIMENTAL METHOD**

#### 1. Composite Material

The composite material investigated in this study was made of S-2 glass fabric and phenolic matrix. Since the fabric was of the plane weave, each piece of fabric could be viewed as unit of [0/90] cross-ply. In making the composite laminate, an angle of 45° was imposed in laying up consecutive pieces of fabric, resulting in quasi-isotropic laminates [0/90/45/-45]<sub>ns</sub>. Mechanical tests were performed to determine the engineering constants. Experimental results are given in Table 1 along with some assumed values (underlined) for computational analysis.

#### 2. Composite Thickness

For a given pin diameter, the composite joint strengths due to bearing failure should be linearly proportional to composite thickness, if the contact conditions between the pin and composites are identical for various composite thicknesses. If not, the stress distributions in the composite laminates will be different, so will be the damage processes. Since contact mechanisms were the primary interests in this study, four composite thicknesses, namely 8-ply, 24-ply, 40-ply, and 80-ply with average thicknesses (H) of 1.93 mm, 5.89 mm, 9.5 mm, and 20.37 mm, respectively, were investigated. In addition, it should be noted that the stacking sequence [0/90/45/-45]<sub>ns</sub> used in laminating composites qualified the thickness increase in a sublimate mode instead of a ply-level mode. The

Table 1: Linear orthotropic material properties determined from experiments and assumed (<u>underlined</u>) for computer simulations.

Young's moduli	$E_{11}' = E_{22}'$	$E_{11}^{\ c} = E_{22}^{\ c}$	E <sub>33</sub>
GPa	11.65	13.17	5.65
Poisson's ratios	$v_{13}^{t} = v_{23}^{t}$	$v_{13}^{ c} = v_{23}^{ c}$	<u>"12</u>
	0.3	0.3	0.3
Shear moduli	$G_{13} = G_{23}$	G <sub>12</sub>	
GPa	2.07	5.03	
Strengths	$X_t = Y_t$	$X_c = Y_c$	
MPa	183.96	134.18	
Bolt bearing strength	$\sigma_h^{\ u}(strength)$	σ <sub>b</sub> <sup>y</sup> (yielding)	
MPa	218.23	153.14	

sublaminate mode was defined as repeating the quasi-isotropic unit [0/90/45/-45] until the desired thickness was reached in composite lamination while the ply-level mode repeated the cross-ply unit [0/90] first then [45/-45], resulting in  $[(0/90)_n/(45/-45)_n]_s$ . Reports, such as Ref. [3], showed that thick section composites based on sublaminate mode gave better properties than their ply-level counterparts.

#### 3. Pin Diameter

Another important parameter for studying contact mechanisms was the pin diameter. The effects of pin diameter on composite joint strength are available for thin composite plates. Those studies were primarily aimed at two-dimensional analysis, i.e. in-plane scaling effect. Very few studies based on three-dimensional analysis are reported. To the authors' best knowledge, thickness scaling effect had not been mentioned. Since the pin diameter was believed to have significant effects on the contact mechanism and stress distribution around hole edge, four different steel pin diameters (D) of 3.125 mm (0.125 in), 6.25 mm (0.25 in), 12.5 mm (0.5 in), and 25 mm (1.0 in) were considered in the present investigation.

#### 4. Composite Mechanical Joint

In this study, a double-lap, single-steel-pin joint as shown in Figure 1 was considered for experimental and finite element model. Since the contact mechanisms between the steel pin and composite and the interaction between the steel pin diameter and

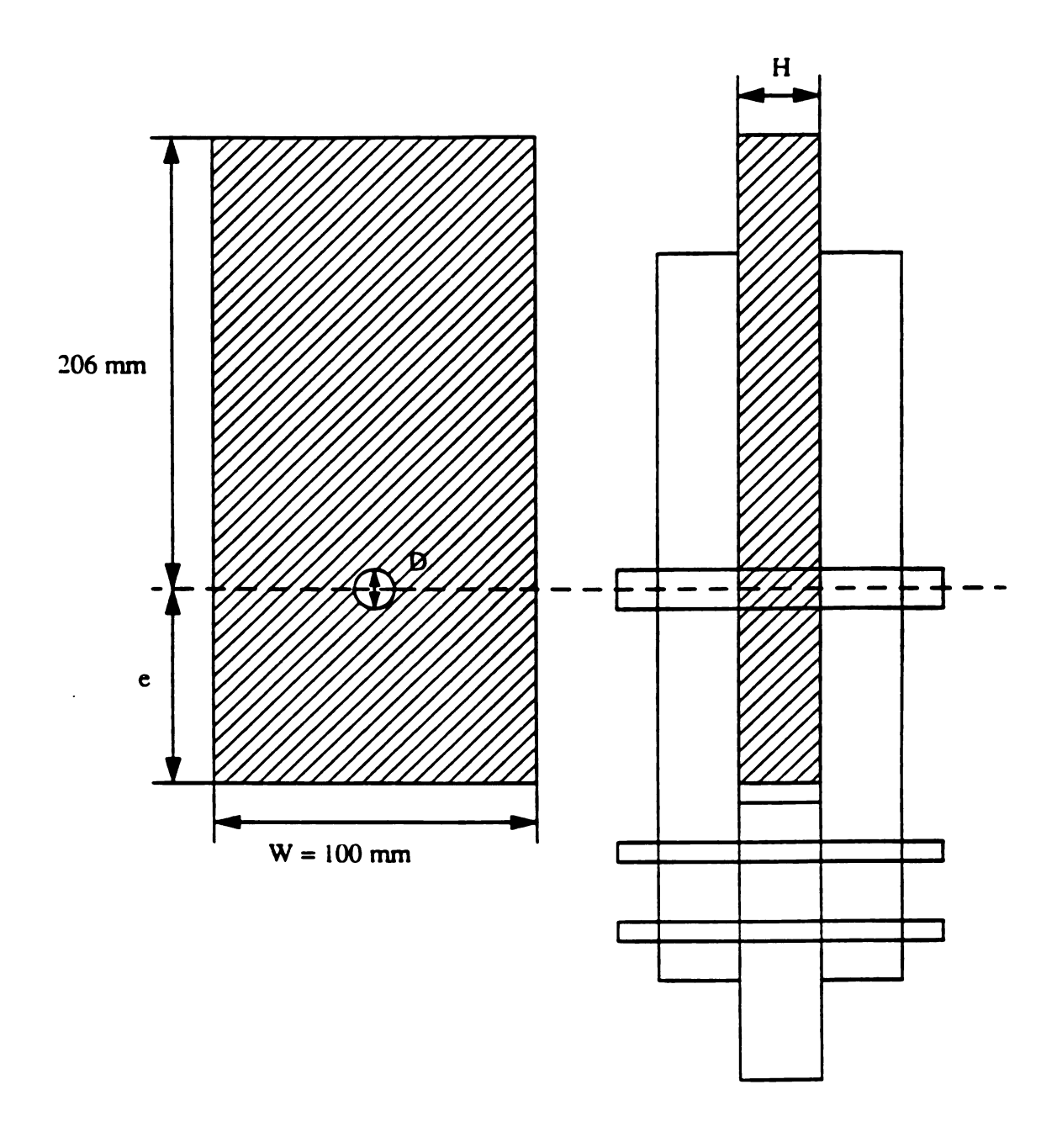


Figure 1 - Schematic diagram for double-lap, single-pin joint.

Table 2: Ratios of  $\frac{W}{D}$ ,  $\frac{e}{D}$ , and  $\left(\frac{H}{D}\right)^2$ .

			8-ply	24-ply	40-ply	80-ply
hole diameter (mm)	$\frac{w}{D}$	e D	$\left(\frac{H}{\overline{D}}\right)^2$	$\left(\frac{H}{D}\right)^2$	$\left(\frac{H}{D}\right)^2$	$\left(\frac{H}{D}\right)^2$
3.125	32	24	0.370	3.445	8.952	41.165
6.25	16	11.75	0.092	0.861	2.238	10.291
12.5	8	5.625	0.023	0.215	0.560	2.573
25	4	2.5625	0.006	0.054	0.140	0.643

composite thickness were the primary focuses for this study, only damage due to bearing failure was of primary interest. Hence, in order to avoid net-section failure from taking place before bearing failure, a relatively large ratio for plate width to pin diameter, i.e. W/D, was required. Regardless of the composite thickness (H), the width (W) for all specimens was fixed as 100 mm (4 in), which was the largest size the tensile grips of the testing machine could accommodate. Accordingly, the W/D ratio were at least 4 or greater for all cases as shown in Table 2.

Similarly, in order to avoid shear-out failure from taking place before bearing failure, the distance from the hole center to the specimen end (e) should be as large as possible. However, it should be pointed out that another important consideration in this study was to minimize the number of composite specimens through using each specimen for all four hole diameters. To begin with, the composite specimens were prepared with 3.125 mm holes by using a carbide drill. The joints were then tested until bearing failure took place. Holes of next size, i.e. 6.25 mm, were then introduced in the failed specimens with the top edges tangent to the existing holes, as shown in Figure 2, to remove the bearing damage around the 3.125 mm hole. The specimens were inspected by X-ray radiography to confirm their integrity before being tested again until bearing failure. If an X-ray radiograph showed extended damage beyond a hole edge, a hole of next size (12.5 mm) was prepared. This process was repeated for holes of 12.5 mm and 25 mm in diameter. Accordingly, the distance from the hole center to the specimen end varied with the hole diameters. The W/D and e/D ratios are summarized in Table 2. For identification purpose, the 16 types of joints made from four thicknesses and four hole diameters, were also given names and are listed in Table 3. The four hole diameters 3.125 mm, 6.25 mm, 12.5 mm,

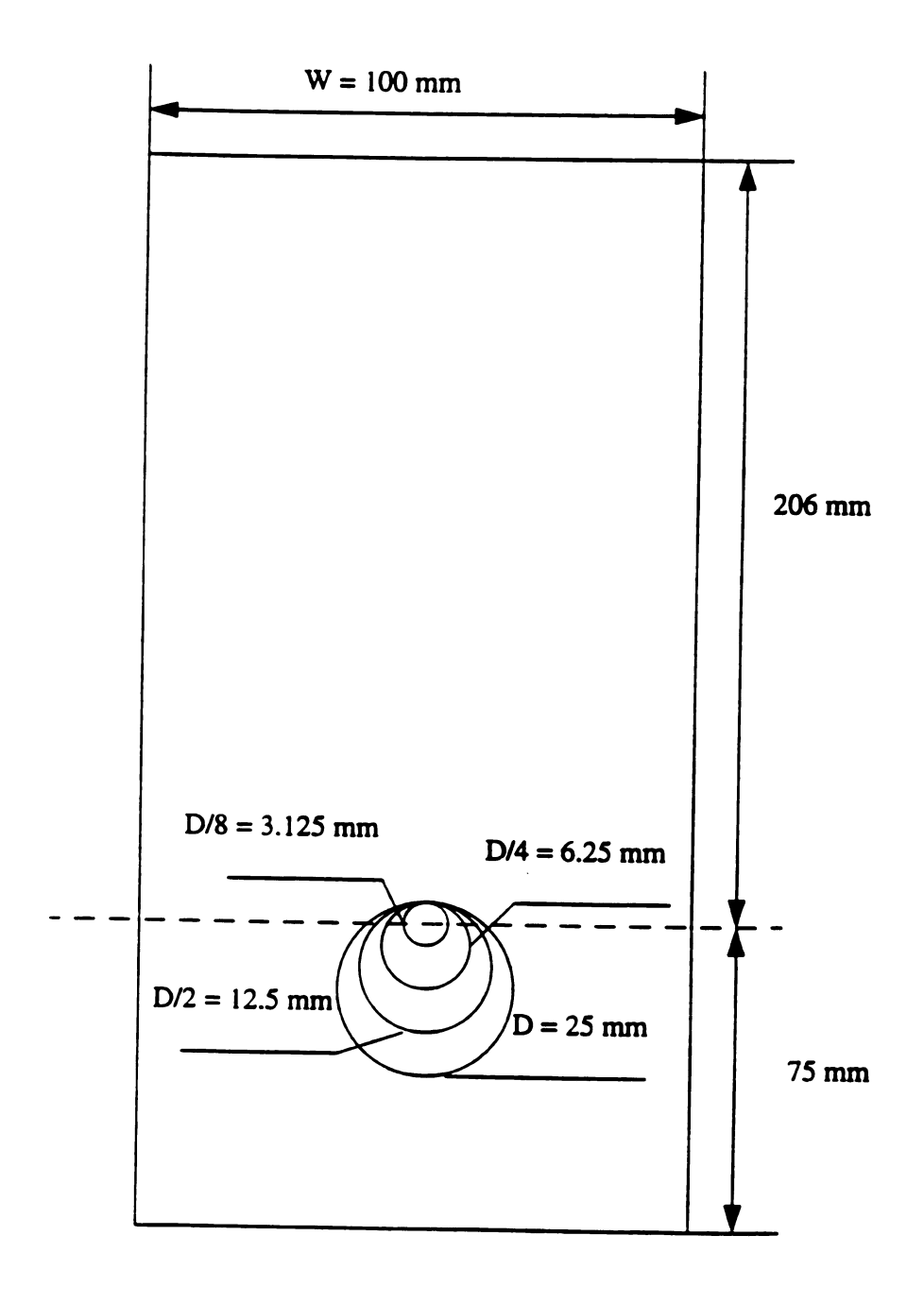


Figure 2 - Progressive hole drilling in composite joint specimen.

Table 3: Specimen nomenclautue for various combinations of pin diameter and plate thickness.

hole diameter	8-ply	24-ply	40-ply	80-ply
3.125	D8H8	D8H4	D8H2	D8H1
6.25	D4H8	D4H4	D4H2	D4H1
12.5	D2H8	D2H4	D2H2	D2H1
25	D1H8	D1H4	D1H2	DIHI

Table 4: Experimental results of joint stiffness and joint stiffness per unit bearing area.

	8-ply	24-ply	40-ply	80-ply
3.125 mm	0.316	0.336	0.216	0.021
Diameter	0.273	0.252	0.220	0.030
	0.440	-	0.097	0.040
Average*	0.343	0.294	0.178	0.030
Efficiency	1.00	0.86	0.52	0.09
Average**	2.069	5.411	5.284	1.910
6.25 mm	0.376	0.267	0.241	0.118
Diameter	0.259	0.284	0.247	0.097
	0.202	0.275	0.218	0.126
	-	0.288	-	-
Average*	0.279	0.279	0.235	0.114
Efficiency	0.81	0.81	0.69	0.33
Average**	3.365	10.271	13.953	14.514
12.5 mm	0.130	0.196	0.184	0.110
Diameter	0.115	0.169	0.179	0.110
	0.119	0.156	0.170	0.096
	-	0.211	0.169	-
Average*	0.121	0.183	0.176	0.105
Efficiency	0.35	0.53	0.51	0.31
Average**	2.919	13.473	20.900	26.736
25 mm	0.102	0.104	0.095	0.057
Diameter	0.103	0.098	0.087	0.059
	0.107	0.100	0.084	0.059
Average*	0.104	0.101	0.089	0.058
Efficiency	0.30	0.29	0.26	0.17
Average**	5.018	14.872	21.138	29.537

<sup>\*</sup> Average joint stiffness per unit bearing area in GPa/mm
\*\* Average joint stiffness in kN/mm

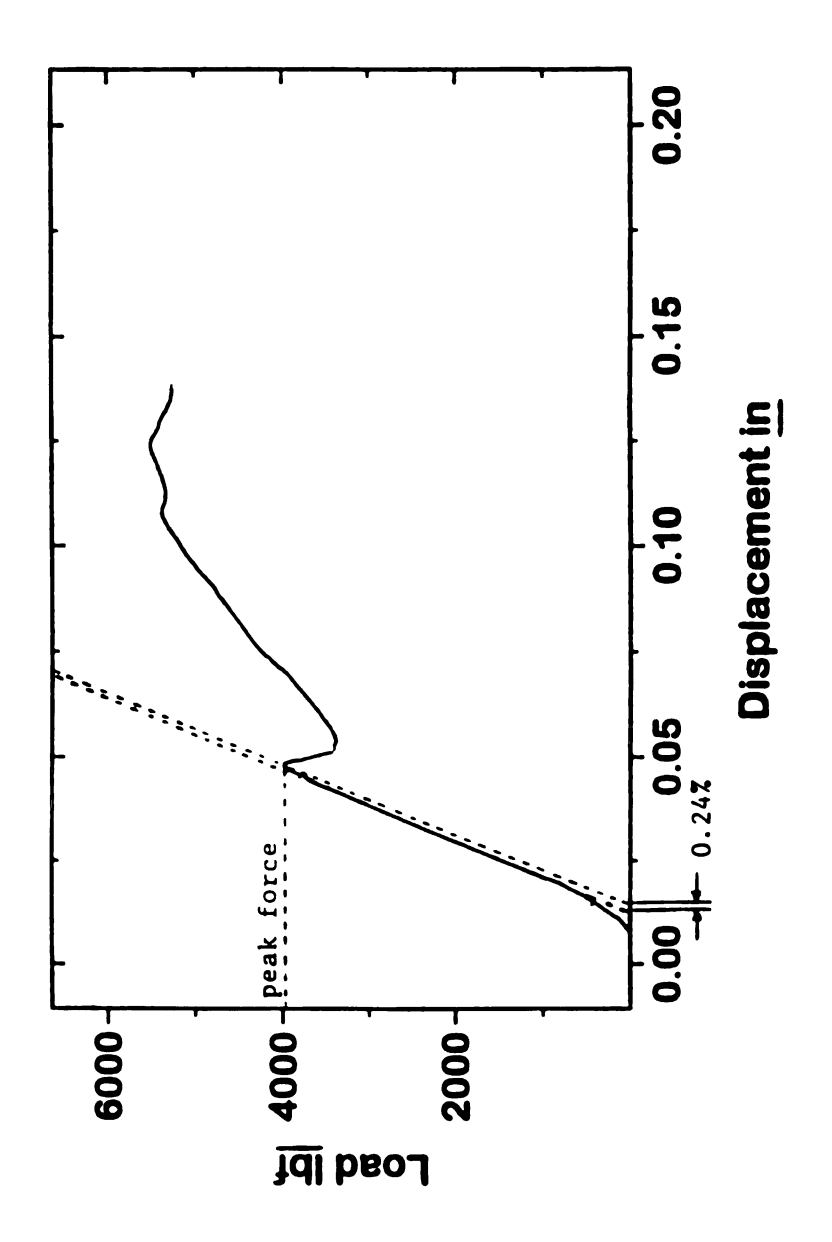


Figure 3 - Load-deformation relation for D2H2, a type A joint.

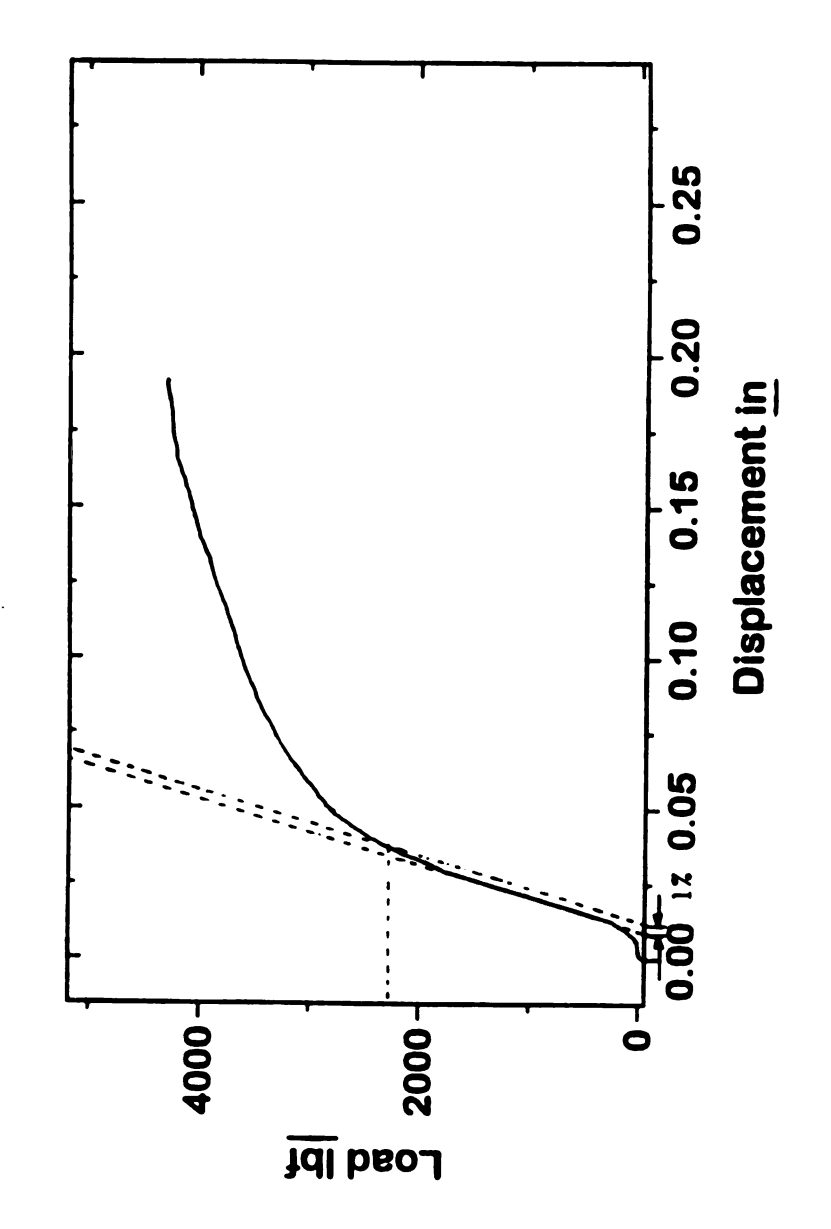


Figure 4 - Load-deformation relation for D4H1, a type C joint.

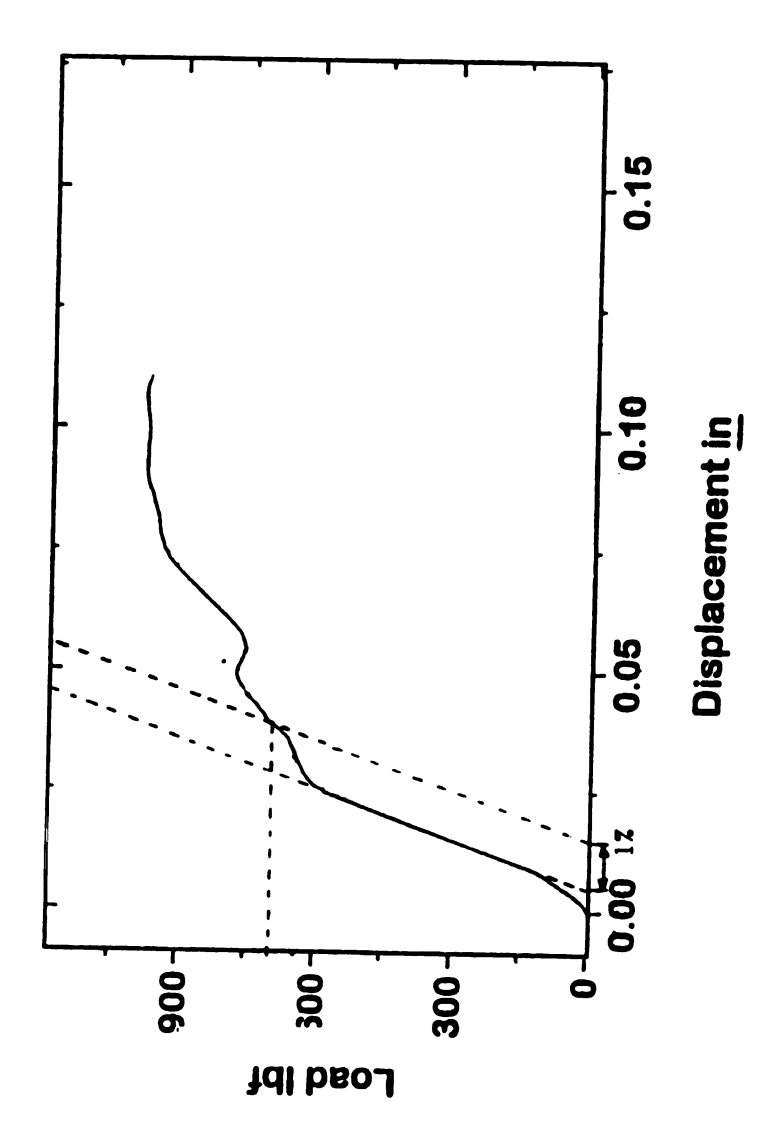


Figure 5 - Load-deformation relation for D1H8, a type B joint.

and 25 mm are designated by D8, D4, D2, and D1, respectively, while the four thicknesses 8-ply, 24-ply, 40-ply, and 80-ply are designated as H8, H4, H2, and H1, respectively. As an example, the composite joint with a hole diameter of 12.5 mm and a laminated thickness of 24-ply is named D2H4.

In addition to W/D and e/D, parameters such as the integrity of hole surface and the clearance between pin and hole also play important roles in composite joining. Since the composite material under investigation was made out of laminates, micro-delamination was likely to take place during hole drilling. Extra care was exercised in hole preparation. X-ray radiographs taken after drilling showed insignificant micro-delamination. In addition, because the pins and composite holes were designed to be snug-fitting, extra care was required in assembling the composite joints.

#### 5. Experimental Results

#### 5.1 Joint Stiffness

Experimental results of joints stiffnesses for all tests are given in Table 4 along with average values. The joints load-deformation curves were determined from the loads measured by Instron testing machine load cell and deformations measured by the LVDT mounted on the hydraulic actuator of the testing machine. The loads and deformations were scanned at every one-tenth of a second. The stiffness of a joint was determined from the slope of the linear portion of the load-deformation curve and is a measure of the rigidity of the joint.

The stiffness were then divided by the corresponding bearing area, i.e. DH, to determine the joint stiffnesses per unit bearing area. Both average values for stiffnesses and stiffnesses per unit bearing area are given in Table 4 for comparisons. Apparently, the stiffness increases as the pin diameter and composite thickness increase except for the cases of D8H2, D8H1, and D2H8. It should be pointed out that these cases are located on the upper right and lower left corners of Table 3.

Another significant result was the efficiency of joint stiffness. also given in Table 4. The efficiencies of joint stiffnesses were obtained by normalizing the average stiffnesses per unit bearing area of all 16 cases with respect to the average stiffness per unit bearing area of D8H8. The D8H8 joint represents a typical thin section joint with matching pin diameter size whose structure behavior is well understood by the researchers. The joint properities of D8H8 were used to normalize the properties of other joints to obtain the efficiencies of the joints. It is noted that all cases have efficiencies lower that D8H8. In fact, the efficiency of joint stiffness seems to decrease as the pin diameter or the composite thickness increases. Besides, it was also found that among the four cases which have relatively similar dimensions between pin diameter and composite thickness, i.e. D8H8, D4H4, D2H2, and D1H1, the efficiency of joint stiffness reduces from 100% for D8H8 to 75% for D4H4, to 47% for D2H2, and to only 15% for D1H1. This result indicates the important role of joint configuration in mechanical joint designs.

#### 5.2 Joint Strength and Bearing Strength

In this study, every composite joint was loaded until bearing failure took place.

The load-deformation relations for all 16 cases can be divided into three categories: type A, type B, and type C. Type A represents load-deformation curve for composite joints having an almost linear load-deformation relation until an abrupt (A for abrupt) loss of load due to bearing failure. The load then picks up again until the ultimate load level is reached. In type C, the linear load-deformation relation continuously (C for continuously) changes into a smooth nonlinear relation without a local maximum or minimum. The third type of load-deformation relation is named type B, which is an intermediate type between (B for between) A and C. Figs. 3-5 show the three types of load-deformation relations, A, B, and C, respectively. The types of load-deformation relation for individual joints are identified and summarized in Table 5.

As mentioned above, every type A joint underwent an abrupt loss of load very close to the end of linear load-deformation relation, and thus had a distinct local peak force. This peak force was considered as the joint strength for type A joints since it matched with bearing failure. Figure 3 shows the load-deformation relation for a D2H2 joint and the peak force. In addition, the offset deformation from the linear range at the peak force could also be identified from the diagram. The offset deformation was then divided by the pin diameter to determine the offset deformation percentage. Results for all type A joints were given in Table 5. It can be seen that the offset deformation percentages for type A joints are all smaller than 1%.

The typical load-deformation relation for type C joints can be found in Figure 4, which is for a D4H1 joint. Apparently, it was difficult to identify the joint strength due to bearing failure since there was no local peak force in the load-deformation relation.

Although there were local peak forces for type B joints, e.g. the load-deformation relation

Table 5: Experimental results of the type of load-deformation relation, joint strength, and offset deformation percentage from linear range.

	8-ply	24-ply	40-ply	80-ply
	type <sup>1</sup> kN <sup>2</sup> % <sup>3</sup>	type kN %	type kN %	type kN %
D/8	A 0.91 0.00 A 0.99 0.00 - 0.95	C 2.65 1.00 C 2.17 1.00	C 3.56 1.00 C 3.12 1.00 C 4.00 1.00 3.56	C 2.53 1.00 C 3.35 1.00 C 2.69 1.00 2.86
average* average** efficiency	0.1553 1.00	0.1286 0.83	0.1180 0.76	0.0442 0.28
D/4	A 1.74 0.16 A 1.54 0.34 A 1.33 0.00	A 6.89 0.69 A 6.55 0.95 A 6.38 1.07 A 6.85 1.20	C 10.90 1.00 C 9.910 1.00 C 9.163 1.00 C 8.006 1.00	C 10.68 1.00 C 10.96 1.00 C 10.17 1.00
average* average** efficiency	1.54 0.1256 0.81	6.67 0.1782 1.15	9.497 0.1574 1.01	10.60 0.0819 0.53
D/2	C 1.94 1.00 A 1.78 0.33 A 1.92 0.60	A 11.12 0.15 A 10.66 0.27 A 10.05 0.33 A 10.78 0.90	A 20.27 0.12 A 18.55 0.36 A 17.57 0.24 A 19.91 0.40	C 35.42 1.00 B 35.24 1.00 B 33.53 1.00
average* average** efficiency	1.88 0.0768 0.50	10.66 0.1424 0.92	19.07 0.1581 1.02	34.73 0.1343 0.86
D	B 3.42 1.00 B 3.08 1.00 A 3.34 0.50 B 3.72 1.00	A 19.57 0.12 A 19.26 0.12 A 18.73 0.17	A 30.69 0.25 A 32.43 0.13 A 31.14 0.13	B 58.84 1.00 B 51.55 1.00 B 51.58 1.00 B 58.94 1.00
average* average** efficiency	3.39 0.0691 0.45	19.18 0.1282 0.83	31.42 0.1302 0.84	55.23 0.1067 0.69

l type of load-deformation relation

<sup>2</sup> joint strength in kN

<sup>3</sup> offset deformation percentage from linear range

<sup>\*</sup> average joint strengths in kN

<sup>\*\*</sup> average joint strengths per unit bearing area in GPa

for a D1H8 joint shown in Figure 5, they were far away from linear ranges. Accordingly, it required a unified definition for determining the joint strength due to bearing failure for all types of joints. Since the offset deformation percentages to bearing failure for type A joints were all smaller than 1%, 1% offset deformation percentage was then used in determining the joint strengths for type B and type C joints. The joint strengths for all cases were identified and are summarized in Table 5. It can be concluded that the joint strength increases as the pin diameter and composite thickness increase except the D8H1 case.

The joint strengths given in Table 5 were also divided by the corresponding bearing area to determine the joint strengths per unit area, i.e.

$$\sigma_B = \frac{P}{DH}$$

where P is the joint strength. Since this actually represents the average stress around the bearing area, it is also called bearing strength. The bearing strengths for all 16 cases are also given in Table 5 along with the efficiencies of bearing strength. The efficiency of bearing strength is defined as ratio determined by normalizing the bearing strength of each case with respect to the bearing strength of D8H8. As can be seen from Table 5, the efficiency of bearing strength remains high for cases close to the diagonal line formed by D8H8, D4H4, and D2H2. However, the efficiency of bearing strength decreases for cases located away from the diagonal line. This result seems to be similar to that observed for the efficiency of joint stiffness to some extent.

The diagonal cases seem to have relatively higher efficiencies of bearing strength than the non-diagonal cases except the D1H1 case which has efficiency of bearing strength of 69%. All joints of D1H1 case have the type B load-deformation relation.

However, by closely examining these curves, they are found to have peak forces corresponding 3% of deformation offset. If the 3% peak forces, instead of those based on 1% deformation offset, are used as joint strengths, the average joint strengths will become 63,949 N rather than 55,226 N, and the efficiency of bearing strength will rise to 80%. This result indicates the critical role of strength definition in mechanical joint analysis.

#### 6. Discussions

### 6.1 Joint Type

Although there are a few exceptions, the type of load-deformation relations for all 16 cases given in Table 5 can be divided into two zones separated by the D8H8-D1H1 diagonal line. Most of the cases located above the diagonal line are of type C while those located on and below the diagnoal line are primarily of type A. The sharp difference of the load-deformation types between the zones is believed to be dependent on the bending rigidity of pins. The upper right zone are joints with thick composites and small pins while the lower left zone are joints with thin composites and large pins. As the loading level increases, the small pins of the upper right zone bend and create highly local contacts with the composites. These contact areas increase and become more uniform through the composite thicknesses as the loading level increases. Accordingly, the type C cases in upper right zone have a smooth nonlinear load-deformation relation following the initial linear relation. In order to identify the type of a composite joints, the following calculation based on strength of materials analysis is proposed.

Consider a pin with a length of 3H (double-lap joint) as shown in Figure 6. The maximum bending stress in the pin can represented by:

$$\sigma_b = \frac{My}{I} = \frac{\frac{(3PH)D}{8}}{\frac{\pi D^4}{4}} = \frac{3PH}{4\pi D^3}$$

which stands for bending stress in the steel pin. A ratio for bending stress t bearing stress can then be defined as

$$\frac{\sigma_b}{\sigma_B} = \frac{3H^2}{4\pi D^2}$$

Table 2 gives the ratio of  $H^2/D^2$  for all 16 cases. The values of  $H^2/D^2$  ratio can be divided into two categories: smaller than unity and greater than unity. In comparison with Table 5, it can be concluded that type A joints have  $H^2/D^2$  ratios smaller than unity while type C joints have  $H^2/D^2$  ratios greater than unity. The type A joints are defined as bearing-mode joints while the type C joints area called bending-mode joints. Since type B is an intermediate type between type A and type C, its failure mode can be either bearing mode or bending mode.

## 6.2 Bending-Mode Joints (Type C Joints)

In the comparison of joint efficiencies, different considerations should be made to different types of joint. For the joints dominated by pin bending mode, the comparison of joint efficiencies should be based on a constant pin diameter. In this case, the joint

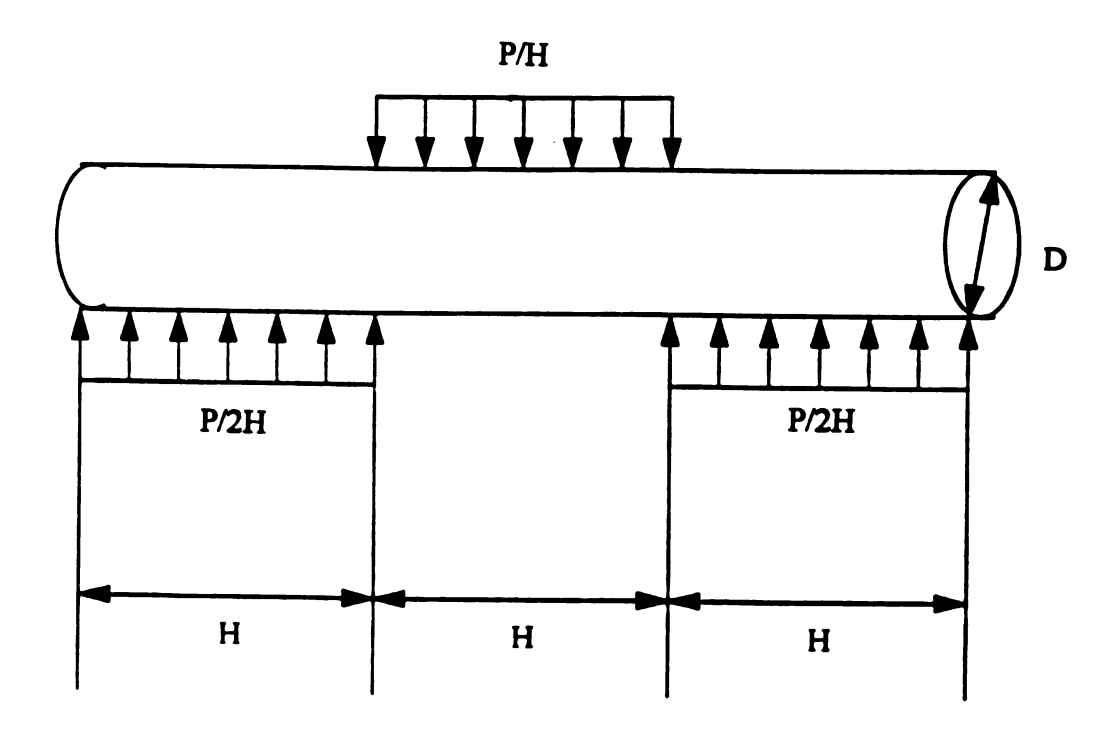


Fig. 6 - Pin subjected to bearing forces.

strengths are expected to increase in proportion to thickness according to

$$P = \sigma_R DH$$

However, the joint strength actually first increases then decreases. In fact, the efficiency of bearing strength decreases as thickness increases. It is believed that the load-deformation curve moves away from linear range as the steel pin indents composite material and causes local bearing failure in composite. Since the strengths of bending-mode joints are defined at 1% deformation offset, the joint strengths are lower for thick composites with small pins due to the premature local bearing failure. In other words, the loading level to cause the local failure does not reflect the total capability of type C joints. As a summary, the efficiency of joint strength is attributed to the two sources: (1) the positive contribution from the increase of bearing area of DH, and (2) the negative contribution due to premature local bearing failure resulting from pin bending. This behavior can be expected for the joint stiffness also.

## 6.3 Bearing-Mode Joints (Type A Joints)

The comparison of joint efficiencies for bearing-mode joints should be made based on a constant composite thickness. In this case, the joint strengths are expected to increase in proportion to pin diameter according to

$$P = \sigma_R DH$$

The joint strength does increase as pin diameter increases; however, the efficiency of joint strength decreases. It is believed that the increase of pin diameter not only provides a larger foundation for supporting a higher joint load but also weakens the integrity of the composite laminates with the associated larger hole. The loss of composite integrity due to the hole size increase has been known as the hole size effect [13]. As a summary, the efficiency of joint strength is attributed to the two sources: (1) the positive contribution due to the pin diameter increase, and (2) the negative contribution due to the loss of joint strength arising from the hole size effect. Similar arguments also hold good for the efficiency of joint stiffness.

## CHAPTER 3 COMPUTATIONAL METHOD

#### 1. Finite Element Method

Although mechanical testing can give both stiffness and strength of a composite joint, it cannot offer any information regarding details of joining characteristics such as the interaction between the pin and the composite and the behaviors of individual elements. In order to gain insight into the behavior of composite joints, e.g. the stress distribution around the hole and the deformed shape of the pin, numerical method is required. In the present study, a very common numerical method, namely finite element method, was used for composite joint investigations. This method is not only useful for studying composite structures with complex geometry, it is also suitable for exploring composite joints with various configurations.

The finite element method is a numerical technique which provides an approximate solution for boundary value problems. It has been used for solving a wide range of engineering and physics problems. Because of its power in solving problems with complex geometry, the finite element method has become a very common technique for computer simulation in solid mechanics. For example, it is a process which is capable of predicting deflections and stresses for a structure subjected to both static and dynamic. In the earliest developments of finite element analysis, quite naturally almost all emphasis was directed toward the development of effective finite elements for the solution of specific problems. However, the potential of the method when used effectively on a digital computer was rapidly realized, and increasingly larger and more complex finite element systems were

considered. This, in turn, enhanced the development of efficient data-handling procedures and effective techniques for the solution of the governing finite element equilibrium equations.

At present, computer programs are in use that can handle at reasonable cost very large finite element systems, because the algorithms employed have been developed specifically for finite element analysis. As a result of this development, when referring to finite element analysis, a complete numerical process implemented on the digital computer is implied.

Three steps should be performed in finite element method of analysis. First, finite element pre-process designs the finite element mesh for the structures or problem investigated, it is called finite element modeling. Finite element modeling is not just a way to make pictures of structure parts and assemblies, it divides the problem geometry into a mesh of elements which are used to calculate the stiffness of the structure and solve for deflections, given the loads and boundary conditions. Second, finite element process performs the finite element analysis to get the solutions for the problem studied. Finite element program development is necessary in this step. Third, finite element post-process analyzes the results from the finite element process, detail stress distribution diagrams, deformation diagram, and single values can be obtained from this post-process, i.e. complex simulation can be readily visualized and understood through post-process.

In this thesis, two commercial codes named FEMB and ABAQUS were involved in the study. The former is a model generator to build finite element mesh while the latter is a numerical solver for finding numerical solutions. That is, in the computer simulation investigation, the finite element modeling software package FEMB was used in the pre-process work, the finite element analysis software package ABAQUS was used in the finite element process work and post-process work.

In the finite element method analysis study, both linear analysis and nonlinear analysis were performed. Since the load-deformation relations were almost linear until bearing failure took place, linear analysis was studied to obtain the detail stress information in the joint structures. In the linear analysis, the composite material was linear orthotropic, and the loading for each case was linearly proportional to the contact area in order to gain identical contact mechanisms for all the cases. Nonlinear analysis was studied to obtain the maximum loading before the bearing failure took place. In the nonlinear analysis, the composite material was nonlinear, and the damage process was performed.

## 2. Finite Element Model

The composite join investigated in computer simulations was modeled as a double-lap, single-steel-pin joint as shown in Figure 7. It is slightly simplified from the real experimental joint configuration as shown in Figure 1. In order to study the scaling effect of pin diameter, four different pin diameters were investigated. In order to study the scaling effect of composite thickness, four different composite thicknesses were investigated. Accordingly, totally 16 cases were investigated in the study of scaling effect. The 16 cases of composite joint, four composite thicknesses and four pin diameters, were assigned names according to these two parameters for identification purpose. Table 3 summarizes the 16 names.

Different combinations of pin diameter and composite thickness will result in different

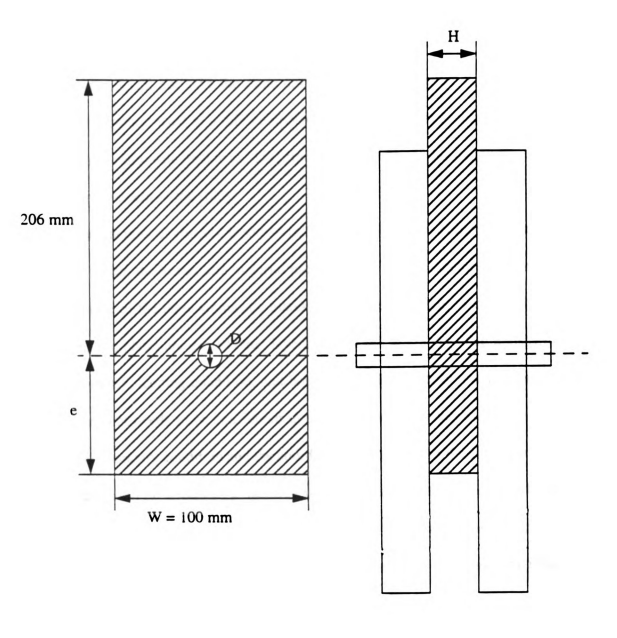


Figure 7 - Schematic diagram for double-lap, single-pin joint in computational method.

contact conditions. Depending on the contact condition, the deformations and stress distributions of the pin and the composite will be different and result in different stiffnesses and strengths for composite joints. For example, a pin with small diameter used in a thick composite material will not have the same uniform stress distribution along the pin as a pin with large diameter used in a thin composite. Accordingly, the scaling effects - both pin diameter and composite thickness - are important issues in composite joining and they are the primary concern of the study.

The composite joint of concern is shown in Figure 7 where three composite plates having the same width, thickness, and material properties are joined together by a steel pin. The middle piece of the three composite plates is called central layer in this study, while the remaining two plates are named outer layers. Due to the symmetry of composite material, joint geometry, loading condition, and boundary condition, only one quarter part of the composite joint needs to be considered in the finite element analysis. Figure 8 gives the symmetric boundary condition and the coordinate system used in the computer simulation. The 1-direction (x-direction) is positive when pointing toward the right side of the composite plate, the 2-direction (y-direction) is positive when pointing toward the top end of the composite plate, and the 3-direction (z-direction) is positive when pointing from the center layer to the outer layer. Also shown in the diagram are the loading direction and fixed boundary condition.

A finite element model generator named FEMB was used to build the finite element mesh of all composite joints. In the process of mesh generation, a structure was divided into a grids of "elements". Each of the elements is a simple shape (in this study, the best design should be cubic), for which the finite element program has information to write the

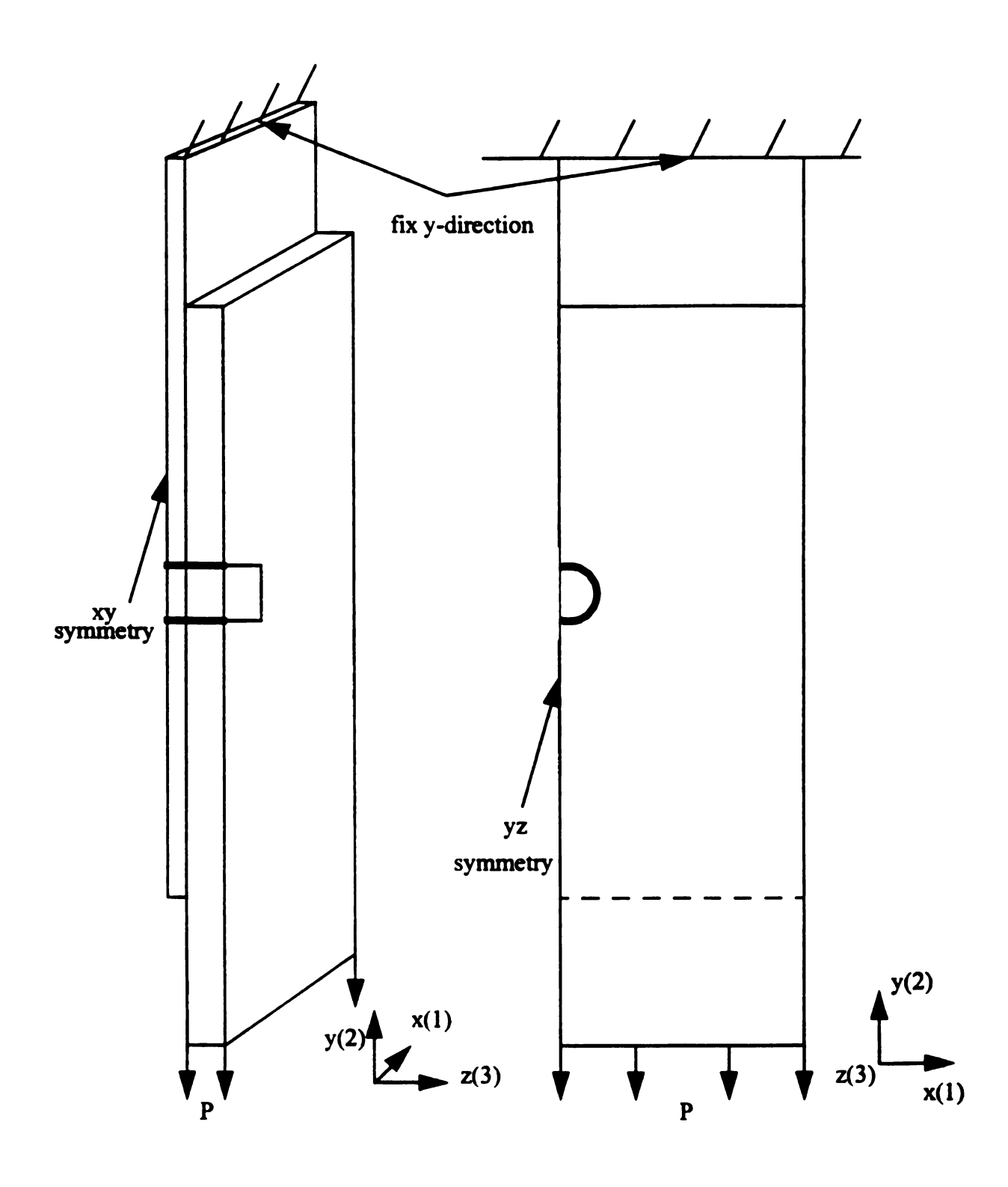


Figure 8 - Symmetric boundary conditions for computer simulation model.

Table 6: Numbers of elements used around the hole edge.

	8-ply	24-ply	40-ply	80-ply
D/8	8	8	8	8
D/4	18	18	18	18
D/2	20	20	20	20
D	30	30	30	30

Table 7: Numbers of layers used in the thickness directions.

	8-ply	24-ply	40-ply	80-ply
D/8	4	4	4	8
D/4	4	4	4	8
D/2	4	4	4	4
D	4	4	4	4

governing equations in the form of a stiffness matrix. The unknowns for each element are the displacements at the "node" points, which are the points at which the elements are connected. The finite element program will assemble the stiffness matrix for these simple elements together to form the global stiffness matrix for the entire model. This stiffness matrix is solved for the unknown displacements, given the known forces and boundary conditions. From the displacements at the nodes, the stresses in each element can be calculated. In FEMB finite element modeling, the basic geometry for the model was built first, then the created "curves", "lines", and "points" were transferred to form the "elements" and "nodes", where the "elements" were connected by "nodes", and the structure mesh was constructed by the "elements" and "nodes".

In light of the three-dimensional models involved in the computer simulations of this study, 8-node solid continuum finite elements were used. There were as many as 16,000 finite elements for most cases. Figure 9 shows the finite element mesh of D1H1 case. Since contact mechanism was the primary study in this computer simulation, the area around the contact surface between the pin and the composite plate needed to be well designed. Shown in Figure 10, the 1, 2, and 3 directions are defined in Figure 7 and Figure 8. The red lines in the Figures indicate the original mesh, and the black ones show the mesh after deformation. Table 6 shows the number of elements around the hole and Table 7 shows the number of layers in the thickness direction for all the 16 cases.

#### 2.1. Material

The composite material properties investigated in the computational study was defined



Figure 9 - The finite element mesh of joint D1H1.

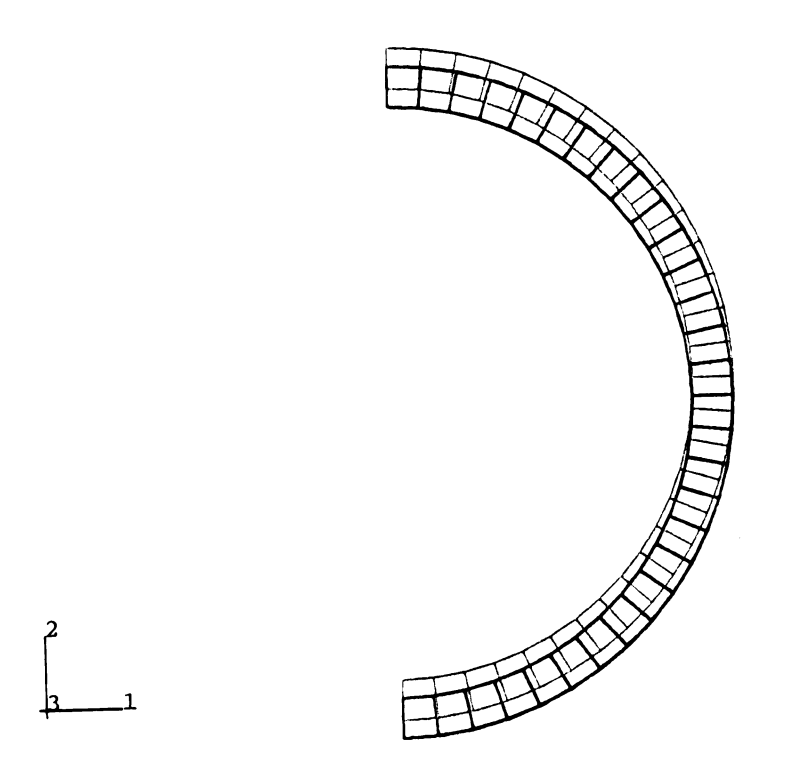


Figure 10 - The finite element mesh around the contact area of joint D1H1.

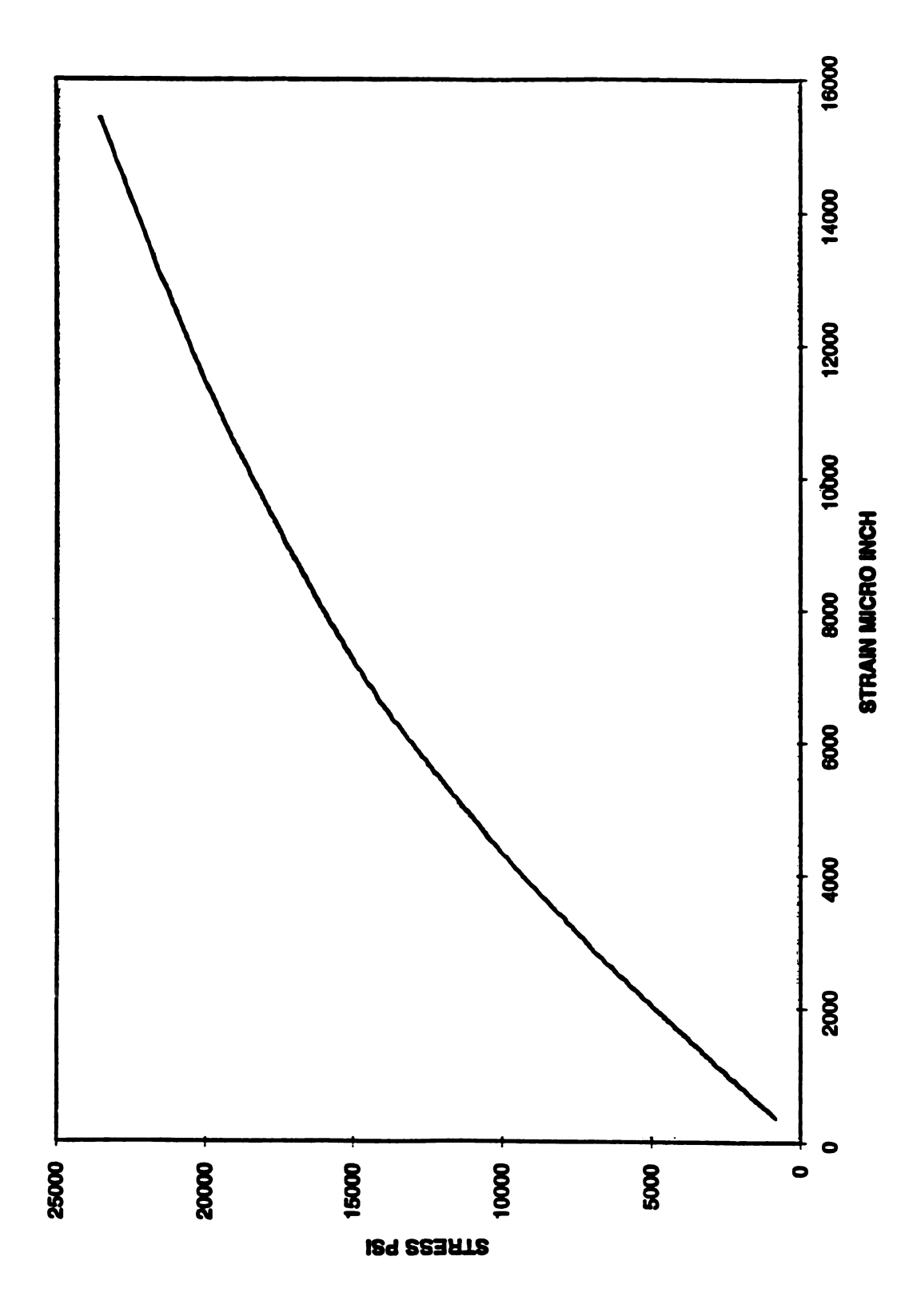


Figure 11 - Nonlinear stress-strain relation of composite material.

from the mechanical test. The linear orthotropic material properties obtained from experiments and used in computer simulations are shown in Table 1. The nonlinear composite material properties investigated was obtained from the mechanical test data as shown in Figure 11. The material model in this computer simulation includes damage, resulting in nonlinear behavior. It also includes various modes of failure, resulting in abrupt loss of stress carrying capacity. The pin material was defined as steel, with Young's modulus of 206.8 Mpa, and Posson's ratio of 0.3.

## 2. 2. Geometry

The composite joint structure in the finite element simulation is shown in Figure 7.

The symmetric conditions of the composite joint structure are shown in Figure 8.

The purpose of finite element model is to make a model that behaves mathematically like the structure modeled, not necessarily one that looks like the real structure. So that the accuracy of the resulting solution will depend on how well the structure was modeled, what type of element used and how fine to make the grid in different areas of the model is. In general, the solution will be more accurate as the structure is subdivided into many fine elements.

In this study, before the investigation of the 16 cases, initial study was done in order to verify the appropriate mesh for this mechanical joint structure. Case D1H1 was performed for this purpose. The reason for choosing case D1H1 is that the area around the hole edge in the composite plates needs more elements to obtain the finer mesh. Since case D1H1 has the largest thickness, it was assumed to be the most difficult one to model. Enough

models for the case D1H1 were designed, and the final solutions from these models were checked to be sufficiently converged, which means the solutions from the computer simulations output were constant. Since the solid brick element used in this composite joint structure modeling are defined to assume that the strain is constant throughout the element, in this study, the fine finite element mesh requires the solid elements to be almost cubic. According to the initial study for the case D1H1, for convenience of generating the 16 cases for computer simulations, four primary mesh were designed. The four primary mesh were based on the same pin diameters, then were scaled in the thickness direction from 2 mm to the other three sizes, 6 mm, 10 mm, 20 mm. For the D8H1, D8H2, D4H1 cases, since the pin diameter sizes are much smaller compared with the composite thicknesses, the new designs were developed for the finer meshes.

## 2. 3. Loading

In this computer simulation, the loading was applied to the bottom ends of the out layers in the downward direction, i.e., along the opposite 2 direction (y direction) in Figure 2, with the central layer fixed on the top end. The pin was snug-fit into the holes of the composite layers.

The loading-deformation relations were almost linear until bearing failure took place. Since contact mechanisms were of the primary concerns in this study, in order to give identical stress distributions in the composite materials and contact conditions, the load-bearing levels of composite materials should be linearly proportional to the contact area between the pins and the composite plates. The distributed loading applied in linear

analysis for each cases are shown in Table 8. Structural loading can be nodal forces (forces directly applied at nodes) or pressures on the face or edge of an element (which are converted to nodal forces internally). In this study, the distributed loading was performed by nodal forces, that is, forces directly applied at the nodes on the bottom ends of the outer layers. Each node was applied the same force to form the distributed loading.

Nonlinear analysis loading model was performed by displacement increment of the cross-head of the outer layer composite plates where the loading was applied. In order to obtain the distributed loading application, it was assumed that all the nodes on the cross-head of the outer layer composite plates, where the loading applied, had the same displacement at the same time. The displacement increment stopped after the bearing failure took place.

# 2. 4. Boundary Condition

In finite element analysis, the boundary conditions are used to build analysis cases containing loads and restraint boundary conditions to apply to the model. An analysis case is a collection of degrees-of-freedom set, constraints, restraints, structural loads, and heat transfer load. In this mechanical composite joint structure, only structural loads and restraints were needed.

In this computer simulation, the nodes on the top end of the central layer were fixed while those on the bottom end of the outer layers were assigned with distribution loading in the downward direction. The structural loads applied here are nodal forces. The restraints were used to restrain the model to match with boundary conditions. Restraints

Table 8: Loading used in finite element linear analysis.

unit: kN

	8-ply	24-ply	40-ply	80-ply
D/8	0.356	1.068	1.779	3.558
D/4	0.712	2.135	3.558	7.117
D/2	1.423	4.270	7.117	14.234
D	2.847	8.540	14.234	28.468

had six values at each node for three translations and three rotations. In finite element model, the restrains were defined to have a value for the fixed displacement, i.e. 0.0 gave the degree fo freedon of no motion. Otherwise, the node was free to move. For example, the nodes on the top end of the central layer had 0.0 value for the 2 direction (y direction). Since the finite element model was of 12 symmetry (xy symmetry), and also 23 symmetry (yz symmetry), the loading applied was of 12 symmetry (xy symmetry), and also 23 symmetry (yz symmetry), it was possible to model only a quarter part of the problem. The symmetric boundary condition definitions were given to the central surfaces, i.e., the nodes on the central surfaces had the restraint definition. Figure 8 shows the symmetric boundary conditions of the finite element model.

#### 2. 5. Contact Surface

In this study, the contact mechanisms of the joint structure were of the most important concern. The scaling effects including the pin diameter scaling effect and composite thickness scaling effect were studied from this contact mechanisms between the steel pin and the composite plates. Therefore the contact interaction was defined between the pin and the composites. Since the loading applied in this composite joint structure was in-plane, there was no need to define the contact interaction between the composite plates, that is, between the central layer composite plate and outer layer composite plates.

The motion of a body at any instant of time may be defined by the linear velocity vector of an arbitrarily chosen point of reference in the body together with the angular velocity vector of the body. Sliding can be defined as the relative linear velocity between the two surfaces at the chosen point. Since the relative linear velocity between the pin and the composite layers was small enough, the small-sliding capability can be used to model the interaction between a deformable body and a rigid body in three dimensions. Small-sliding contact surface was defined between the pin and the composite layers. Figure 8 shows the contact surfaces in bold line.

With the small-sliding contact approach in this mechanical joint structure, the steel pin surface was defined as "master" surface and the composites hole surface as "slave" surface. A kinematic constraint that the slave surface nodes do not penetrate the master surface was then enforced. The contacting surfaces need not have matching meshes; however, the best accuracy was obtained if the meshes are initially matched. Detailed contact stresses information were then obtained from computer simulation.

## 3. Finite Element Analysis

#### 3. 1. Linear Analysis

Linear analysis was performed in the study since the stress-strain relation of the composite material was almost linear until bearing failure took place, this analysis provided detail stresses information of the composite joint structure. It should be pointed out that the stresses information obtained from ABAQUS, the computational analysis were the Cauchy stresses.

In this linear static analysis, the composite material properties were linear orthotropic, and the loadings applied were distribution loading. In this structural problem, the initial configuration of the structure and its deformation throughout the history of loading can be described clearly through this linear analysis. Detail information about the contact stresses along the contact surface between the steel pin and the composite plates, and in-plane stresses in the whole composite structure were obtained from this analysis. The joint stiffnesses and joint strengths of the composite joint structure were defined through these information. Then the mechanical composite efficiencies for all the 16 cases can be concluded from these results.

## 3. 2. Nonlinear Analysis

Because of the geometric discontinuity involved in the mechanical joints, the stress distribution is expected to be highly concentrated around the holes. The high local stress concentration can cause isolated damage to the composite joint while the majority of the joint remains intact. Accordingly, damage analysis is necessary for a complete simulation. The nonlinear analysis which included nonlinear orthotropic material properties and damage process was performed to find the allowable loading in individual joint cases.

Failure modes in composites are strongly dependent on geometry, loading direction, and ply orientation. Failure modes can be divided into in-plane failure modes and transverse failures modes (associated with interlaminar shear and interlaminar normal stresses). Experimental results showed that the major damage mode was of bearing mode, which was essentially attributed to delamination. In order to include delamination modeling laminate analysis, interlaminar stresses need to be calculated. However, this will become almost impossible since it requires many layers in the thickness direction to represent

laminate interfaces. This process can exhaust the computation quickly. Although it is possible to introduce a refined plate theory for interlaminar stress analysis, it does not exist in the current version of ABAQUS. As a compromise of taking advantage of the availability of ABAQUS and honoring the fact of bearing damage, the bearing damage is considered as compressive damage in computer simulation. Accordingly, in-plane failure modes are considered. Therefore, five failure modes can be considered: matrix tensile cracking, matrix compression, fiber breakage, fiber matrix shearing and fiber buckling. Since the contact area in the composite plate was loaded in compression, all of the above five mechanisms, with the exception of fiber breakage are relevant to compression failure in the composite joints.

The strength properties for the composite plates were obtained from mechanical test, and were shown in Table 1. The strength parameters can be combined into Chang-Lessard failure criteria [33]. The sharp load drop-off in the numerical results later discussed was due to the lack of residual stress carrying capacity after the failure criterion is exceeded. In the model analyzed here, four different failure modes are considered.

1. Matrix Tensile Cracking: It can occur due to a combination of transverse tensile stress, and shear stress. The failure index can be defined in terms of these stresses and the strength parameters. When the index exceeds 1.0, failure is assumed to occur. The failure index takes the form

$$e_m^2 = \left(\frac{\sigma_v}{Y_t}\right) + \frac{\frac{2\sigma_{xy}^2}{G_{xy}} + 3\alpha\sigma_{xy}^4}{\frac{2S_c^2}{G_{xy}} + 3\alpha S_c^4}$$

2. Matrix Compressive Failure: It can occurs due to a combination of transverse compressive stress and shear stress. The failure criterion has the same form as for matrix tensile cracking:

$$e_m^2 = \left(\frac{\sigma_v}{Y_c}\right) + \frac{\frac{2\sigma_{xy}^2}{G_{xy}} + 3\alpha\sigma_{xy}^4}{\frac{2S_c^2}{G_{xy}} + 3\alpha S_c^4}$$

The same failure index is used since the above two failure mechanisms cannot occur simultaneously at the same point. After the failure index exceeds 1.0, both the transverse and shear stiffness of the ply drop to zero, and stresses can only be carried in the fiber direction.

3. Fiber-matrix Shearing Failure: It occurs due to a combination of fiber compression and matrix shearing. The failure criterion has essentially the same from as the other two criteria:

$$e_{fs}^2 = \left(\frac{\sigma_x}{X_c}\right) + \frac{\frac{2\sigma_{xy}^2}{G_{xy}} + 3\alpha\sigma_{xy}^4}{\frac{2S_c^2}{G_{xy}} + 3\alpha S_c^4}$$

This mechanism can occur simultaneously with the other two criteria, and, hence, a separate failure index is used. After the failure index exceeds 1.0, shear stresses are no longer supported, but direct stresses in the fiber and transverse directions continue to be supported.

4. Fiber Buckling Failure: It occurs when the maximum compressive stress in the fiber

direction exceeds the fiber buckling strength, independent of the other stress components:

$$e_b = -\frac{\sigma_x}{X_c}$$

It is obvious that, unless the shear stress vanishes exactly, fiber-matrix shearing failure occurs prior to fiber buckling. However, fiber buckling may follow subsequent to fiber shearing, because only the shear stiffness degrades after fiber-matrix shearing failure. Fiber buckling in a layer is a catastrophic mode of failure. Hence, after this failure index exceeds 1.0, it is assumed that the material at this point can no longer support any loads.

In this computer simulation, loading was carried by incremental displacement of the cross section of the composite plates where the loading was applied. The failure occurred when anyone of the failure indexes which were mentioned above exceeded 1.0. See Figure 12 for the nonlinear damage computer simulation process.

In this study, it is assumed that once failure occurs, the stresses in the damaged directions drop to zero immediately. In reality, the load carrying capacity degrades gradually with increasing strain after failure. Hence, the behavior of the composite after onset of failure is not likely to be identified accuratly by this model. Moreover, the instantaneous loss of stress carrying capacity also makes the post-failure analysis results strongly dependent on the refinement of the finite element mesh and the finite element type used.

#### 4. Computational Results

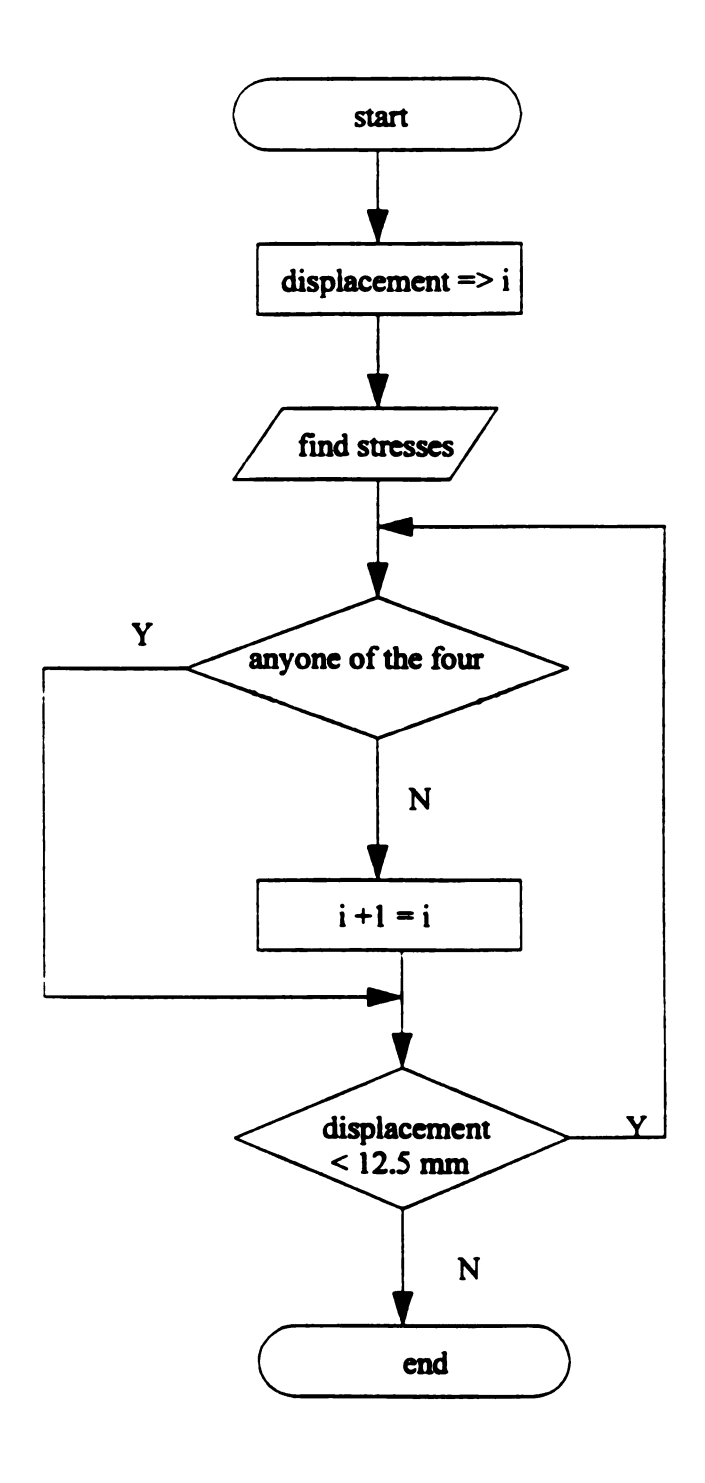


Figure 12 - Nonlinear analysis computer simulation process.

#### 1. Deformation

Figure 9 shows the original mesh in red color, and the mesh after the deformation in black for case D1H1 from linear analysis in front view, which is perpendicular to the xy plane, see Figure 8 for directions. From this diagram, it is seen that the outer composite layers and the central composite layer except the top surface have been moved downward. Apparently, it is the reasonable result from this linear static analysis.

Color diagram of Figure 10 gives the original mesh which is around the contact area in red color, and the mesh after the deformation in black for case D1H1 from linear analysis in front view, which is perpendicular to the xy plane, see Figure 8 for directions. It gives a clear view on the deformation of the mesh around the contact area.

The contact surfaces of the composite plates which initially match the pin contact surface before and after the deformation for the case D1H1 has been shown in color diagram of Figure 10, also in front view, where the red color shows the original surface and the black one shows the surface after the deformation. It obviously shows that the contact surfaces of the composite plates have been moved downward. The reason of showing D1H1 case here is that it have relatively more elements around the contact surface than other cases, so it may give better deformation behavior around the contact area of the composite structure.

Figure 13 shows the deformation of the pin for case D8H1, which gives the clear view for the bending behavior of the steel pin after the deformation. This case has the largest thickness and the smallest pin diameter among the 16 cases. The deformation of the pin after bending can be seen clearly.



Figure 13 - Bending behavior of the pin in joint D8H1.

Table 9: Bending behavior of the pin after deformation from linear analysis.

	8-ply	24-ply	40-ply	80-ply
D/8	5.98*	54.67	121.80	289.52
D/4	1.00	12.42	39.05	136.67
D/2	0.00	5.00	8.50	40.25
D	0.00	0.00	1.50	8.25

<sup>\*</sup> modified by mutiplying 10<sup>4</sup>

Bending behavior of the pin does exist in this mechanical composite structure. Table 9 shows the information of the bending behavior for all 16 cases. The values in this table are the sine values of the angles between the very bottom line on the pin contact surface before the deformation and after the deformation.

The sine values of the angles between the bottom line on the pin surface before the deformation and after the deformation were obtained from the following equation:

$$\theta = \sin^{-1} \left( \frac{displacement2 - displacement1}{thickness} \right)$$

where the displacement 1 is the displacement of the node which at the central end of the bottom line on the pin surface, while displacement 2 is at the outer end in the finite element mesh, and thickness is the thickness of the composite plates in each case.

From Table 9, the results report that the bending behavior of the pin in the composite plates holes are different with the different pin diameter size and composite thickness. The angle change is not proportional to the pin diameter and composite thickness change. It will increase as the pin diameter decreases, while increases as the composite thickness increases.

## 2. Contact Stresses

Since the contact mechanisms were of the primary concern in this computer simulation, contact stresses were studied carefully for all 16 cases in the finite element linear analysis. See color diagrams Figure 14 for the contact normal stresses (cpress) of case D1H1, Figure 15 for the contact shear stresses in the 1 direction (shear1) of case D1H1, and Figure 16 for the contact stresses in the 2 direction (shear2). The 1 and 2 directions are x, y directions and are shown in Figure 8. From the color diagrams, it has obviously shown that the maximum value of contact normal stresses between the pin and the composite plate is not right at the central bottom point of the composite hole edge. Since the bottom sides of the two composite outer layers were under the loadings in the downward direction, i.e., the y or 2 direction in Figure 8, and the top side of the central composite layer was fixed in the opposite of the loading direction, it is believed that the maximum contact normal stress should be approximately at the central bottom point of the hole edge in the central composite layer. In fact, due to the bending behavior of the pin, which was put right through the composite holes, the maximum contact stresses locations was different with the different pin diameter and composite thickness design in this composite joints.

Table 10 shows the locations of the maximum bearing stresses for all 16 cases, which are indicated by the angles and thickness proportions. The angles here are between the yz plane and the line which is connected by the center of the pin circle and the location where the maximum bearing stress happened on the xy plane, see the diagram below the Table 10. The thickness proportions are the z coordination where the maximum bearing stress happened divided by the thickness of the composite plates for each case. Since the loading was applied on the bottom ends of the outer composite layers, and the top end of central composite layer was fixed. The contact surface between the pin and the composite plates were under compressive loading, and the maximum contact bearing stress would be on the contact surface between the pin and the central composite plate for sure. So that the thickness proportion in Table 8 can be considered in another way, that is, 0 means the

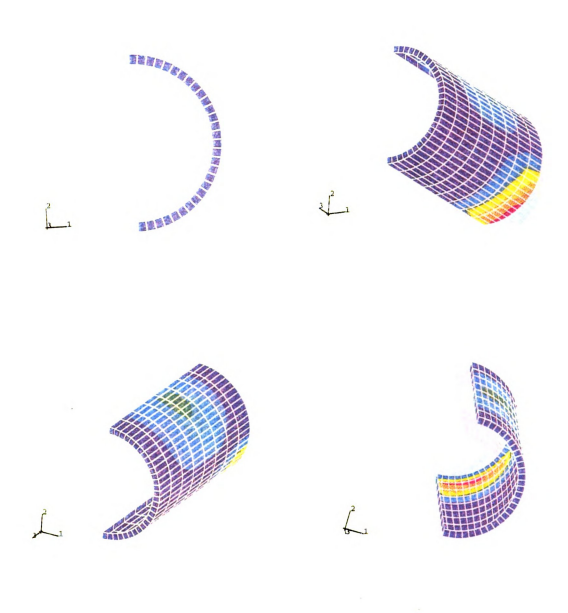


Figure 14 - The contact normal stresses on the pin contact surface for joint D1H1.

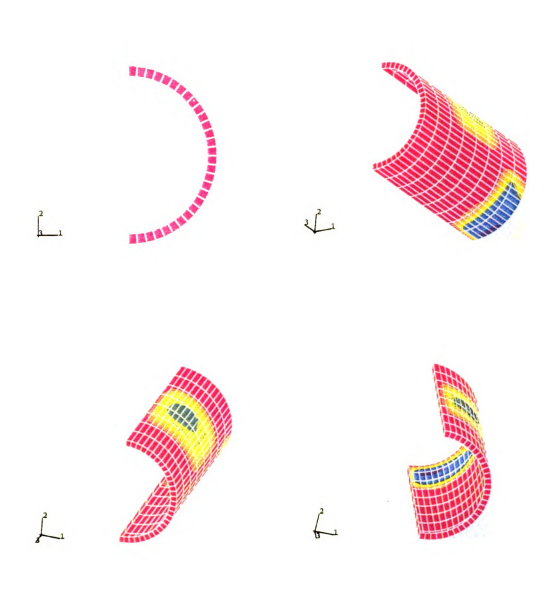


Figure 15 - The contact shear1 stresses on the pin contact surface for joint D1H1.

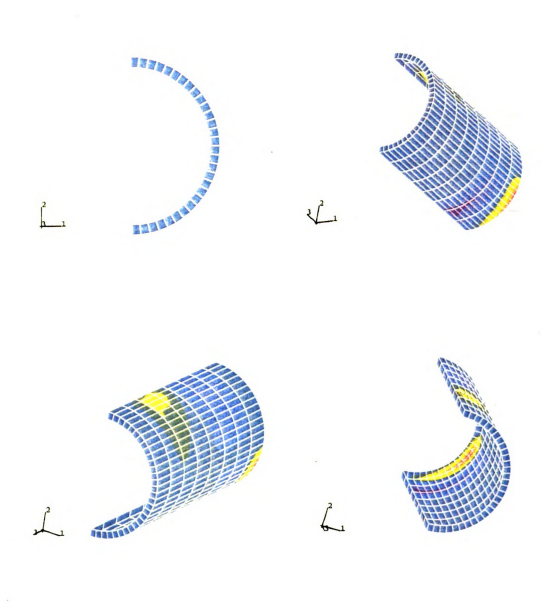
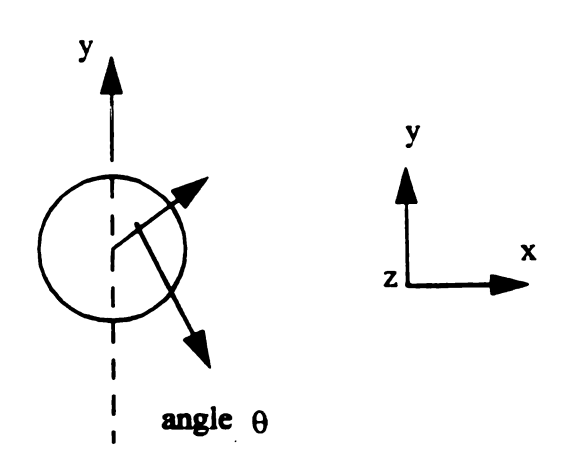


Figure 16 - The contact shear2 stresses on the pin contact surface for joint D1H1.

Table 10: Computed results of the node numbers and locations in polar coordinates for the maximum bearing sresses.

	8-ply	24-ply	40-ply	80-ply	
D/8	D/8 22.5118*		22.5118	22.5118	
	0.5**		0.5	0	
D/4	18.0091	18.0091	35.9989	18.0091	
	0.25	0	0	0	
D/2	20.0101	20.0101	20.0101	20.0101	
	0.25	0.25	0	0	
D	30.0152	30.0152	30.0152	30.0152	
	0.25	0.25	0.25	0	



\*\* z/h

location is right at the plane of the inner end of the central composite plate in the finite element model, and 0.25 means the location is right at the central plane of the central composite plate in the finite element model, and 0.5 means the location is right at the plane of the outer end of the central composite plate in the finite element model.

From Table 8, it can be seen that the location of the maximum bearing stress has the tendency to move from outer end of the central composite plate to the inner end of the central composite plate as the composite thickness increases. And the location of the maximum bearing stress has the tendency to move from outer end of the central composite plate to the inner end of the central composite plate as the pin diameter increases. This result wil provide a valuable basis on designing thick composite joint structures.

### 3. In-plane Stresses

The computer simulation also gives the in-plane stress distributions in the whole structure. Take central composite plate as a example, Figure 17 shows the normal tensile stresses, which are the stresses along the 1 direction of case D1H1, Figure 18 shows the S12, which is the shear stress of case D1H1, Figure 19 shows normal compressive stresses, which are the stresses along the 2 direction of case D1H1 in different view point. The 1, 2 and 3 directions are defined in Figure 8.

These diagrams give the detailed information of the in-plane stresses in this composite joint structure after the deformation. It should be noted that these results of in-plane stresses distribution can only obtained from the finite element linear analysis.

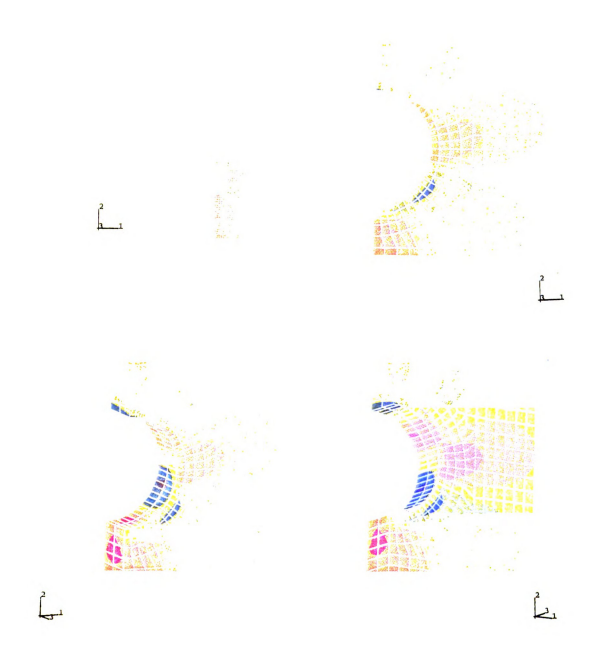


Figure 17 - The in-plane tensile stresses of the central composite plate for joint D1H1.

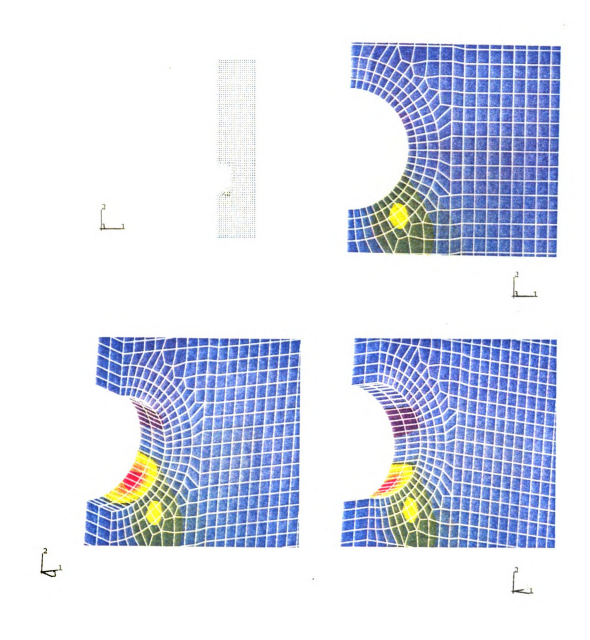


Figure 18 - The in-plane shear stresses of the central composite plate for joint D1H1.

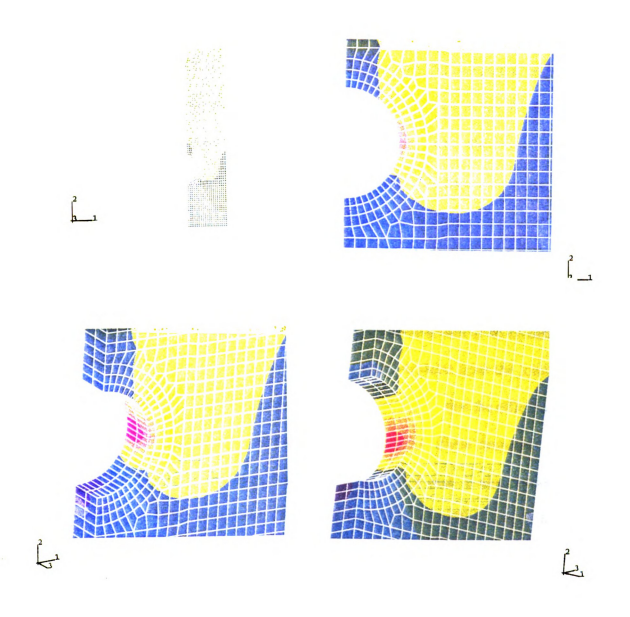


Figure 19 - The in-plane compressive stresses of the central composite plate for joint D1H1.

## 4. Joint Stiffness

Computational results of joint stiffnesses for all cases are given in Table 11. The joint stiffnesses were obtained from the loading divided by the displacement of the composite outer layers ends where the loading applied in the computer simulations, and from dividing the forces output from the load cell by the cross-head movement in experimental investigations. It obviously shows that the joint stiffness increases as the pin diameter and composite thickness increase except the cases of D8H1 and D8H2. The change of the joint stiffness is not linearly proportional to the thickness or the pin diameter change. It should be noted that the cases D8H1 and D8H2 are located on the upper right corner of the Table 11.

Table 11 also gives the results of the efficiencies of joint stiffnesses. The efficiencies were obtained from normalizing the stiffnesses per unit bearing area of all 16 cases by that of D8H8, where the joint stiffnesses per unit area were obtained from the joint stiffness divided by the corresponding bearing area-DH. The results show that the efficiencies of all cases are lower than case D8H8, and the efficiency of joint stiffness decreases as the pin diameter or the composite thickness increases except D8H8 case. It also shows that the efficiency of joint of the four cases, D8H8, D4H4, D2H2, and D1H1, which have relatively similar dimensions between pin diameter and composite thickness, reduces from 100% for D8H8 to 57% for D4H4, to 32% for D2H2, and to only 16.9% for D1H1. It indicates that the joint configuration is playing an important role in mechanical joint design.

The computer simulation result of thickness scaling effect, which is based on constant pin diameters, matches the mechanical test result. But the computer simulation result of

Table 11: Joint stiffnesses from both experiments and computations.

unit: kN/mm

	8-ply	24-ply	40-ply	80-ply
D/8 efficiency	2.899	7.661	6.938	4.419
	(2.309)*	(5.547)	(5.398)	(1.980)
	1.00	0.88	0.47	0.15
D/4 efficiency	3.385	10.02	15.92	20.276
	(3.452)	(10.52)	(14.31)	(14.78)
	0.58	0.576	0.55	0.35
D/2	3.842	11.41	18.53	35.56
	(3.002)	(13.56)	(21.36)	(27.40)
efficiency	0.33	0.327	0.32	0.31
D efficiency	3.983 (5.512) 0.171	11.83 (15.32) 0.170	19.63 (21.69) 0.169	38.40 (29.68) 0.166

<sup>\*</sup> experimental results in parentheses

in-plane scaling effect, which is based on constant composite thickness, matches the mechanical test result except case D2H8. The reason for this mismatch is probably because that the finite element mesh is not fine enough. This reason may also be applied to explain the discrepancy between the computer simulation results and the mechanical test results. It should be pointed out that more elements used for finer finite element mesh will result in more computer memory. Due to the limit of the computer resource, proper finite element mesh was designed in this computer simulation study. The comparison of the joint stiffnesses between the computer simulation and the mechanical test is shown in Figure 20.

# 5. Joint Strength

Computational results of joint strengths for all cases were given in Table 12 along with the experimental results. The joint strengths in the computer simulations were obtained from the multiplying of the yielding stress by the loading. The combined value was then divided by the maximum contact normal stresses, i.e.

$$strength = \frac{153.14}{mcpress} \times loading$$

where the yielding stress of 153.14 MPa determined from an independent bearing test was used as the strength to bearing failure, and mcpress is the maximum contact normal stresses obtained from the contact stresses output from the computer simulation.

Table 12 also gives the results of the efficiencies of the joint strengths. The efficiencies were obtained from nomalizing the joint strengths per unit bearing area of all 16 cases

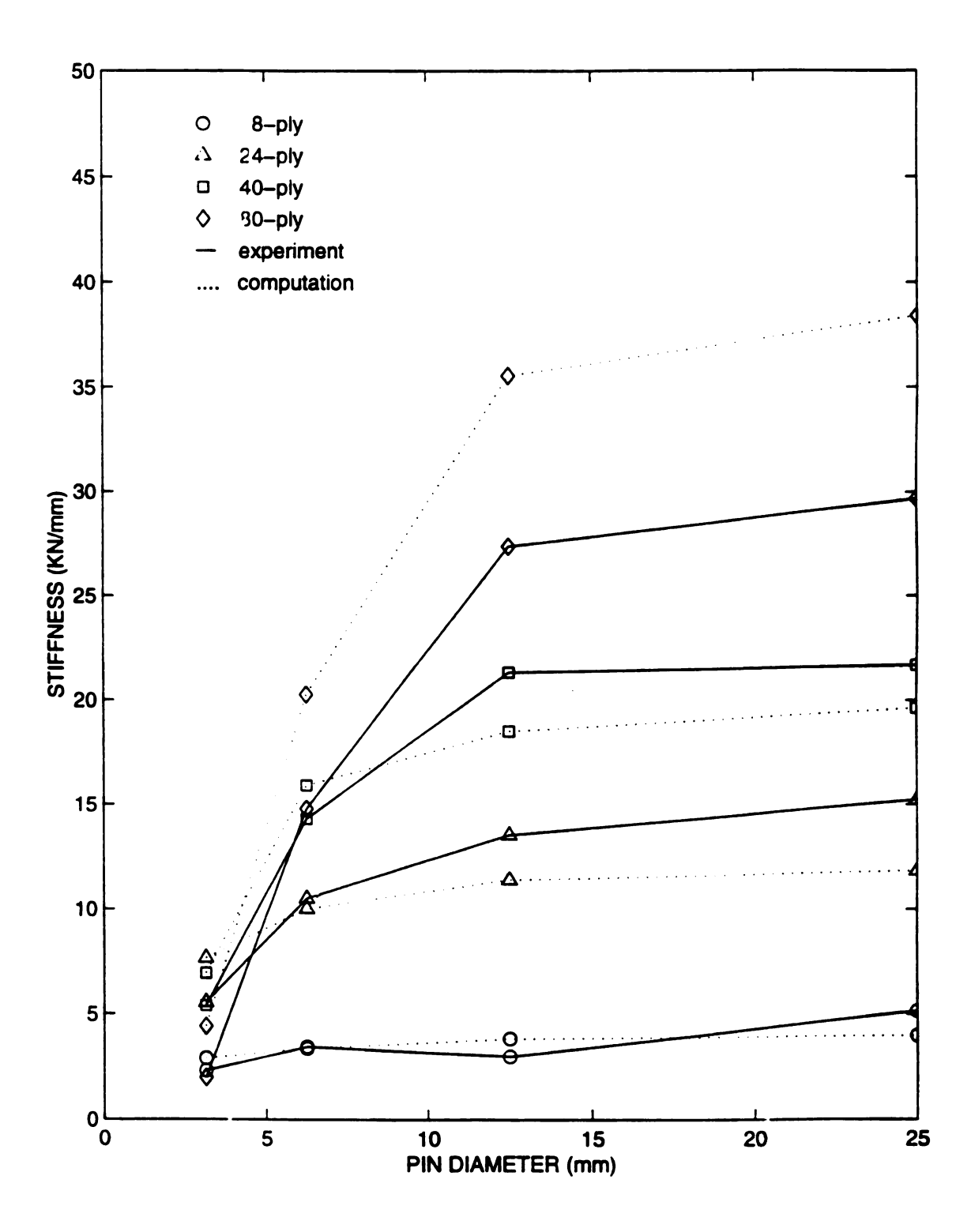


Figure 20 - Comparison of joint stiffnesses.

Table 12: Joint strengths from both experiments and computations.

unit: kN

	8-ply	24-ply	40-ply	80-ply
D/8	0.792	2.678	2.945	3.901
	(0.952)*	(2.406)	(3.558)	(2.860)
	1.000	1.170	0.773	0.527
D/4	1.597	4.795	7.909	8.807
	(1.539)	(6.668)	(9.497)	(10.600)
	1.048	1.050	1.039	1.158
D/2	3.145	10.004	17.218	35.264
	(1.882)	(10.657)	(19.073)	(34.730)
	1.033	1.095	1.131	1.158
D	6.196	20.007	34.472	59.283
	(3.390)	(19.184)	(31.416)	(55.226)
	1.017	1.093	1.094	0.794

<sup>\*</sup> experimental results in parentheses

by that of D8H8. The joint strengths per unit bearing area were obtained from dividing the joint strengths by the corresponding bearing area-DH, i.e.

efficiency= 
$$\frac{153.14}{mcpress} \times \frac{loading}{D \times H}$$

where D is the pin diameter, and H is the composite thickness of the mechanical composite joint structure. Figure 21 shows the comparison of joint strengths between the experimental results and computational results.

# 6. Damage Analysis

Reduced integration element type, which uses a lower order integration method to form the element stiffness, was applied in the nonlinear damage analysis in order to gain more accurate results. Load-displacement curve for case D1H1 is shown in Figure 22. It shows that the load-displacement relation is nonlinear due to the nonlinear stress-strain relation in composite plates and damage process. The maximum forces for all 16 cases are shown in Table 13. It is defined that the failure occurs right at the maximum loading and the peak-force in load-displacement curve is the maximum loading of the composite joint.

The maximum loading can be applied to this double-lap, single-pin mechanical composite joint, which was defined as joining strength increases as the pin diameter and the composite thickness increase. See Table 13. The joining strengths change with different pin diameter and composite thickness, but not proportional to the pin diameter and composite thickness.

The efficiencies for the joining strength were also shown in Table 13. The efficiencies

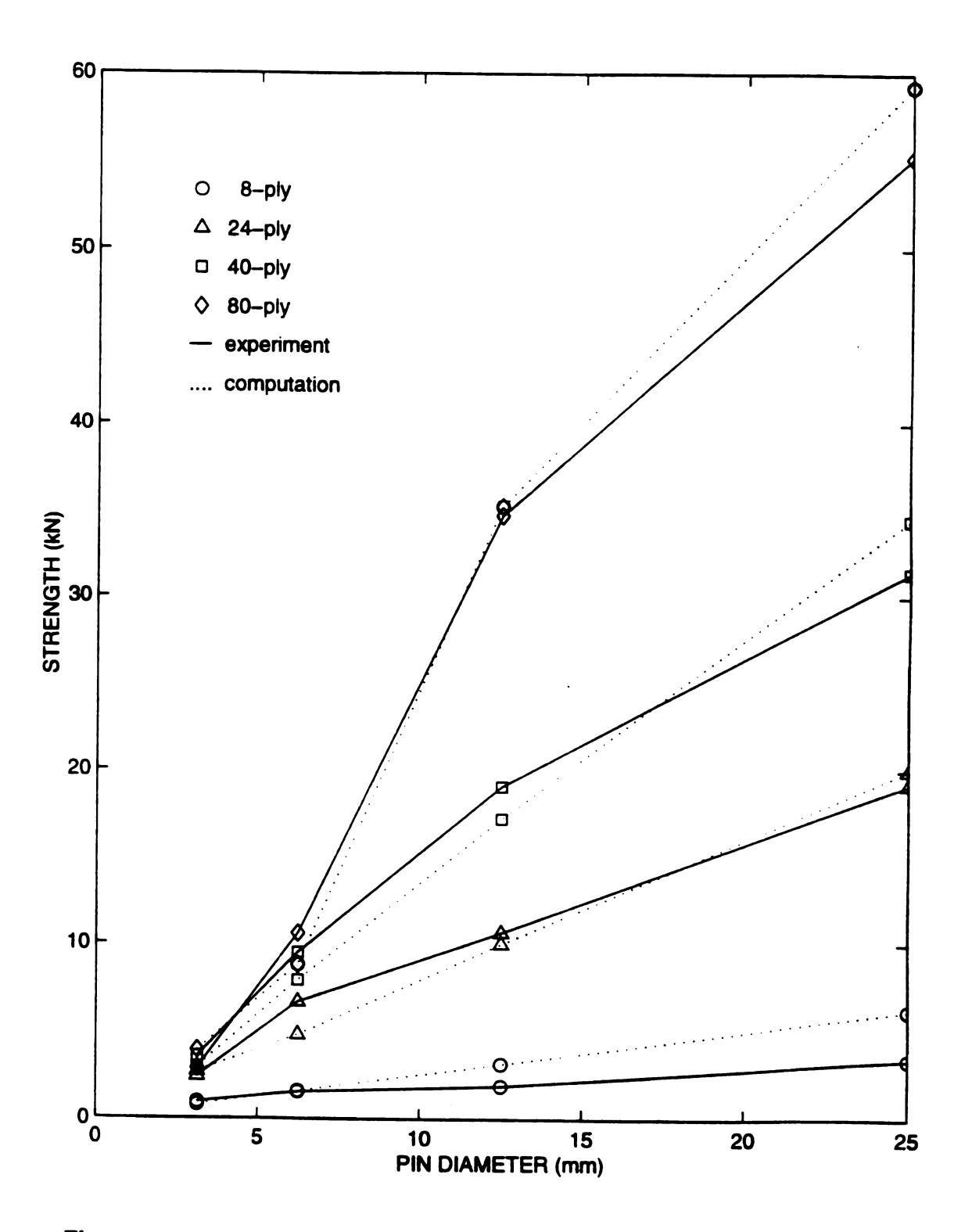


Figure 21 - Comparison of joint strengths.

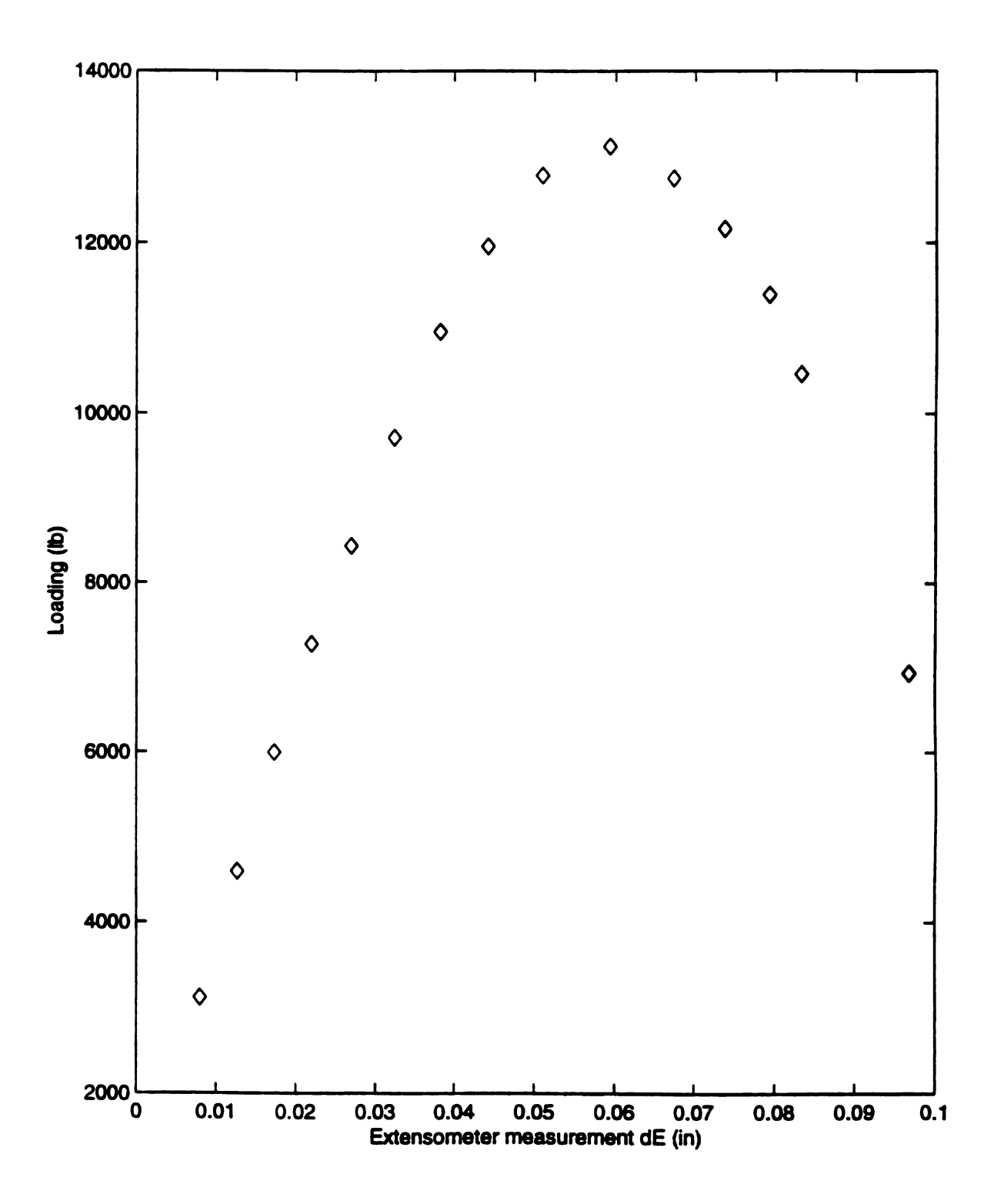


Figure 22 - Load-deformation relation of joint D1H1 from computational results.

were obtained from the joining strengths divided by the corresponding contact bearing area, then normalized by dividing that of the case D8H8. The result shows that the efficiency of all cases are lower than that of the case D8H8, and the efficiency of the maximum load applied decreases as the pin diameter or the composite thickness increases. The comparison of the joining strengths between the nonlinear computer simulation results and the experimental results is shown in Figure 23.

The discussions for efficiencies of joining strength in the nonlinear analysis can be carried out the same way as the linear analysis. That is, the 16 cases investigated here should be divided into two composite joint mode, one is bearing-mode joint and the other is bending-mode joint. The bearing-mode joints have relatively large pin diameter and small composite thickness, and should be discussed based on constant composite thickness. The results give that the efficiency of joining strength decreases as the pin diameter increases. The bending-mode joints should be discussed based on constant pin diameter. The results give that the efficiency of joining strength decreases as the composite thickness increases.

The load-displacement curve in the computer simulations drops off sharply after the maximum loading is reached as discussed earlier. This is due to the lack of residual stress carrying capacity after failure. It should be pointed out that the results from computer simulation are strongly depended on the finite element mesh. Figure 24 shows the extended damage in the central composite plate at the maximum loading for case D8H1. Layer 1, 2, 3 and 4 are the finite element layers from the inner to outer. Damage initially took place at the location where the stress concentration located, and then propagated along the contact area between the pin and the central composite plate. From Figure 24, it can be found that

Table 13: Joint strengths from experiments and nonlinear computations.

unit: kN

	8-ply	24-ply	40-ply	80-ply
D/8 efficiency	0.832	2.523	3.001	3.459
	(0.952)*	(2.406)	(3.558)	(2.860)
	1.000	1.011	0.721	0.416
D/4 efficiency	1.594	5.893	8.706	9.358
	(1.539)	(6.668)	(9.497)	(10.600)
	0.958	1.181	1.046	0.560
D/2 efficiency	2.792	10.187	17.992	35.073
	(1.882)	(10.657)	(19.073)	(34.730)
	0.834	1.020	1.081	1.054
D efficiency	5.617 (3.390) 0.0844	19.799 (19.184) 0.9915	33.846 (31.416) 1.017	58.384 (55.226) 0.877

<sup>\*</sup> experimental results in parentheses

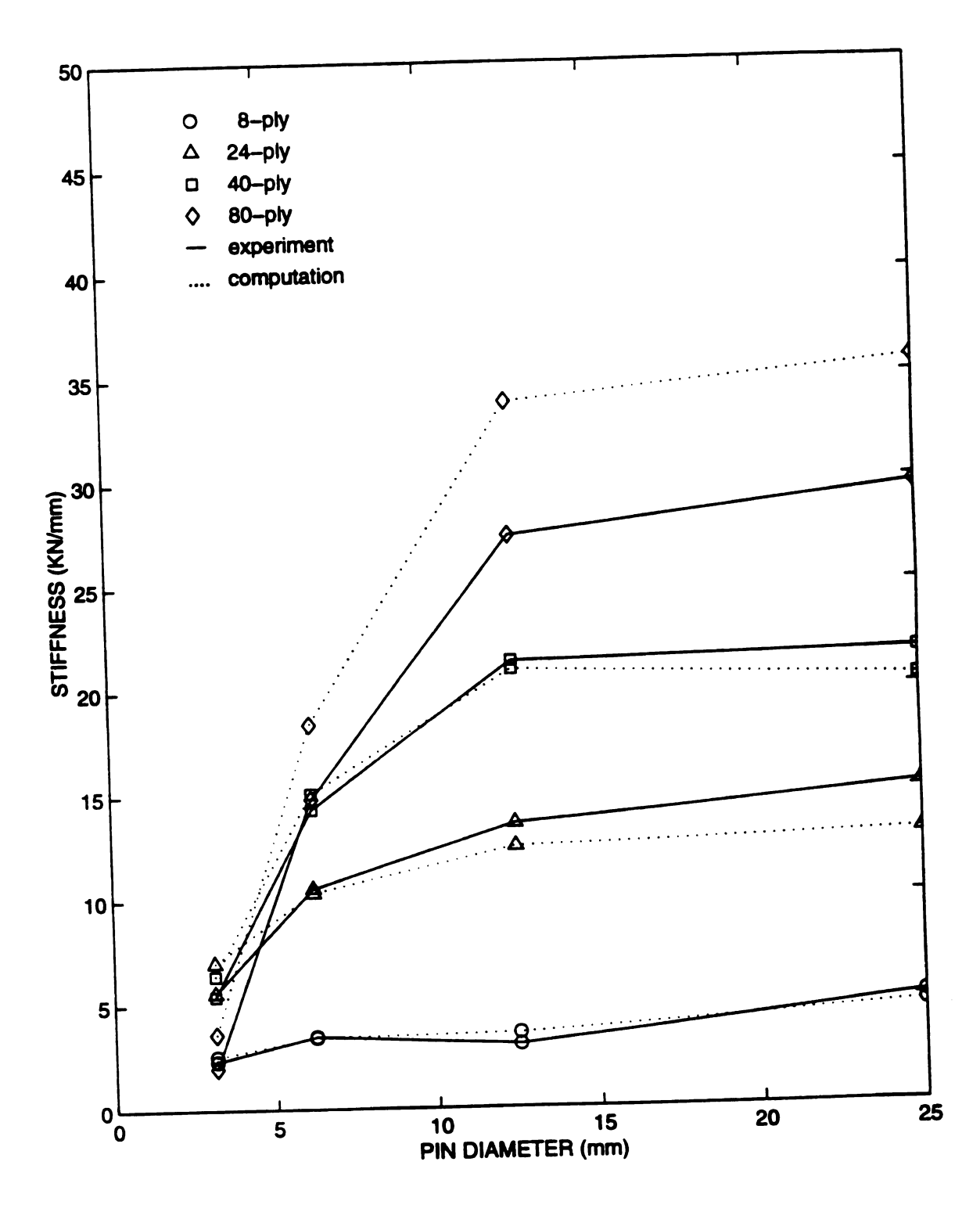


Figure 23 - Comparison of joint strengths.

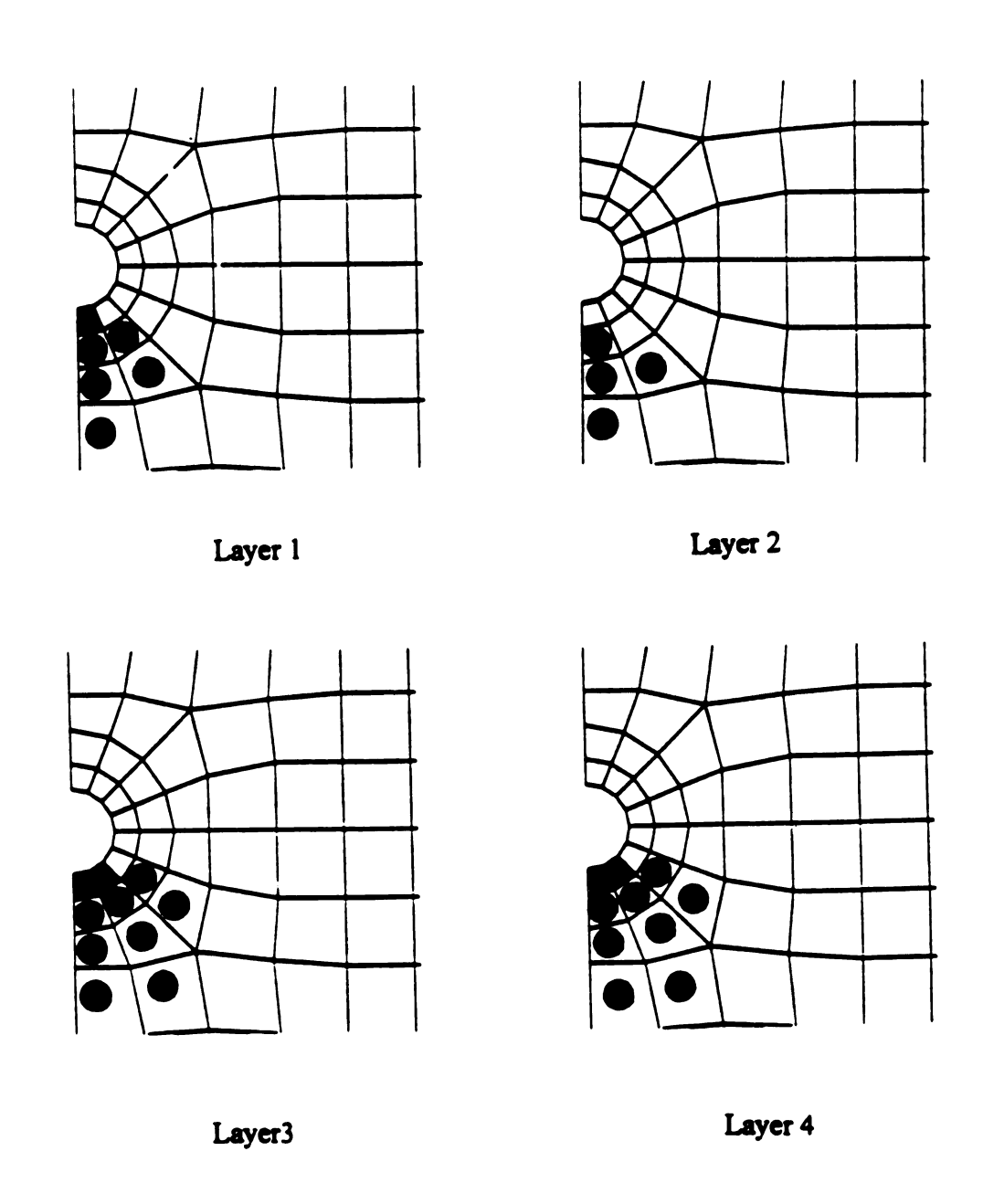


Figure 24 - Extended damage of D8H1 joint.

the damage occurs around the hole edge at the outer part of the composite plate. It is believed that the relatively small pin diameter and the large thickness of this case are attributed to the bending behavior.

The joining stiffness is actually the slope of the linear part of the load-deformation curve. Table 14 gives the joining stiffness for all 16 cases. The discussions for the joining strength are feasible to the joining stiffness, i.e. the 16 cases investigated can be divided into two composite joint mode. Bearing-mode joints have relatively large pin diameter and small composite thickness, and should be discussed based on constant composite thickness. The results give that the efficiency of joining stiffness decreases as the pin diameter increases. Bending-mode joints have relatively small pin diameter and large composite thickness, and should be based on constant pin diameters. The results give that the efficiency of joining stiffness decreases as the composite thickness increases. Figure 25 shows the comparison of the joining stiffness between the experimental results and the nonlinear computer simulation results.

Table 14: Joint stiffnesses from experiments and nonlinear computations.

unit: kN/mm

	8-ply	24-ply	40-ply	80-ply
D/8	2.542 (2.309)*	6.983 (5.547)	6.372 (5.398)	3.590 (1.980)
efficiency	1.00	0.91	0.50	0.14
D/4	3.397 (3.452)	10.31 (10.52)	15.07 (14.31)	18.39 (14.78)
efficiency	0.67	0.68	0.60	0.36
D/2	3.539 (3.002)	12.45 (13.56)	20.96 (21.36)	33.83 (27.40)
efficiency	0.35	0.409	0.413	0.33
D	4.752	12.97	20.38	35.68
efficiency	(5.512) 0.23	(15.32) 0.21	(21.69) 0.20	(29.68) 0.17

<sup>\*</sup> experimental results in parentheses

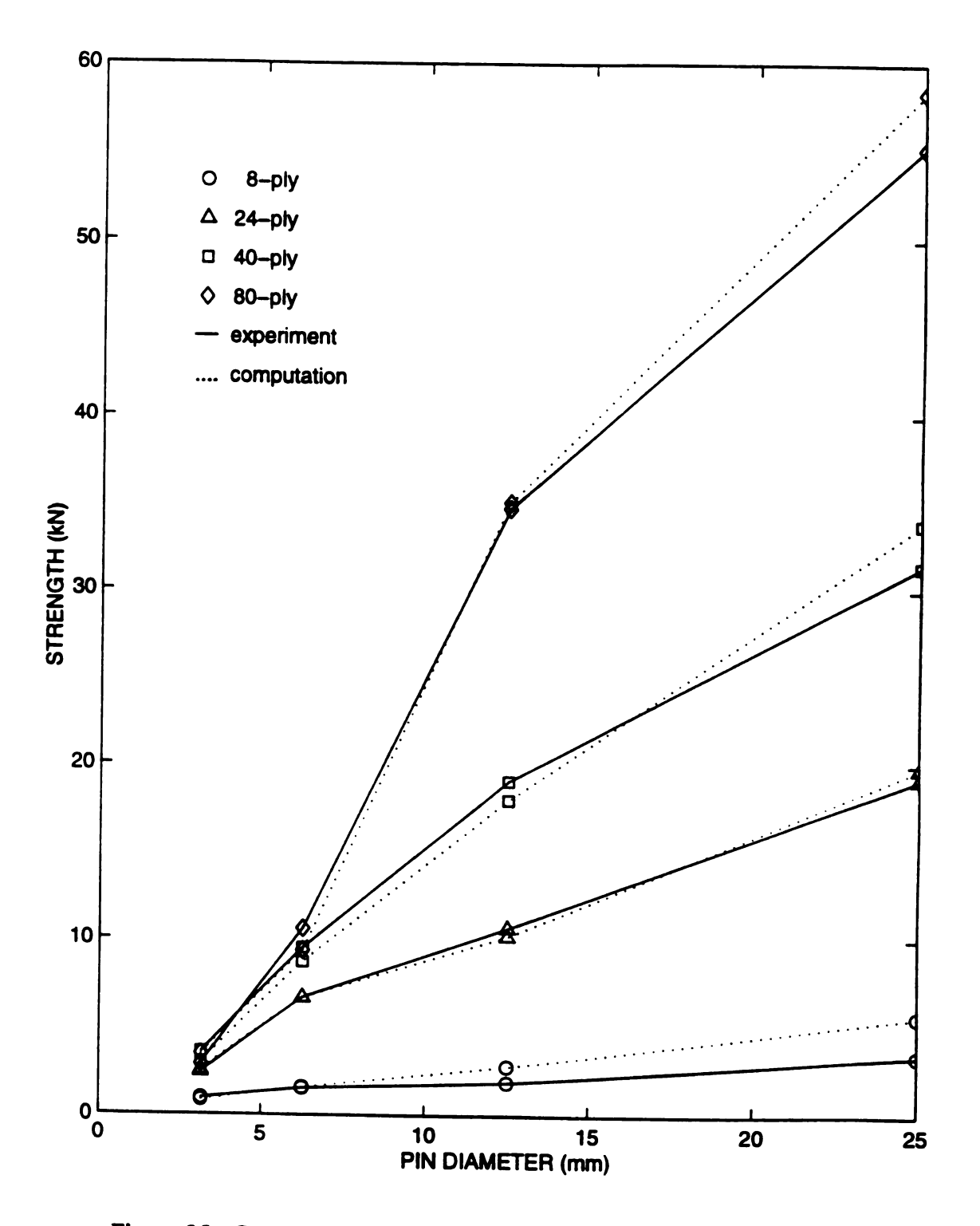


Figure 25 - Comparison of joint stiffnesses.

#### **CHAPTER 4 CONCLUSIONS AND RECOMMENDATIONS**

#### 1. Conclusions

The following conclusions could be drawn from both experimental and computational studies:

- 1. The bending behavior of the pin does exist in mechanical composite joints. The location of the maximum contact-bearing stress in the composite joints, which is considered as the starting point of damage process, is strongly affected by the bending behavior of the pin. The results of the bending behavior of the pins for all 16 cases investigated contribute to the thick composite joints design.
- 2. The linear analysis and nonlinear damage process based on the compression failure model have been used to characterize the mechanical composite joints. The joint stiffnesses, the joint strengths, the stress distribution in the joint structure can be obtained from the investigations. Definitions for the joint stiffness and joint strength in both experimental investigation and computer simulation were developed in this thesis.
- 3. The joint stiffnesses and joint strengths for all 16 cases are not proportional to the bearing area. In other words, both the joint stiffnesses per unit bearing area and the joint strengths per unit bearing area are different for various cases. These results indicate that there exist different contact mechanisms for the cases investigated. It is to say that thick-

ness scaling effects do exist in mechanical joints.

- 4. The contact mechanisms for all 16 cases investigated can be divided into two categories: bending-mode and bearing-mode. Most of the cases located above the diagonal line formed by D8H8 and D1H1 cases belong to bending mode while the remaining cases belong to bearing mode. The ratio of  $H^2/D^2$  can be used to distinguish the types of contact mode. A composite joint with  $H^2/D^2$  greater than unity, a bending-mode contact between the pin and composite is likely to take place. Otherwise, the contact mode will be essentially of the bearing-mode.
- 5. The comparisons of joint efficiencies can be separated into two categories according to the type of the joint mode. For the cases dominated by bending-mode, the comparisons should be based on constant pin diameters. Both efficiencies of joint stiffness and joint strength decrease as the composite thickness increases. It is believed that the joint stiffness and joint strength should increase in proportion to the thickness increase. However, the increasing rates are hindered by the premature local failure due to the bending of small pin in thick composite.
- 6. The comparisons of joint efficiencies for bearing-mode joints should be based on constant composite thicknesses. Both efficiencies of joint stiffness and joint strength decrease as pin diameter increases. It is believed that the joint stiffness and strength should increase in proportional to the pin diameter increase. However, the increasing rates are hindered by the hole size effect, i.e. the reduction of composite integrity due to the hole diameter

increase.

- 7. From the nonlinear damage process, maximum loading for each case can be found. The maximum loading was defined as the loading where the damage to occur in the composite plates, and was studied as joining strength in this thesis. Initially, damage took place at the location where the stresses are highly concentrated. It then propagated along the bottom area on the contact surface between the pin and central composite plates.
- 8. In addition to the low efficiencies in stiffness and strength, the finite element simulations for composite joints made of thick plates with small pins and thin plates with large pins also experience large numerical discrepancies when compared with experimental results. It is believed that the larger differences between the pin diameter and composite thickness in these two cases require much finer mesh for finite element analysis.

#### 2. Recommendations

From the comparisons between computer simulations and experimental investigations, it is found that the results from the finite element simulations bear some degree of error. The possibility for the discrepancy between computer simulation and experimental investigations is due to the coarse finite element meshes used in the study. Finer finite element mesh are needed for the future work.

Although experimental technique can give both stiffness and strength of the mechanical fasteners, it is not able to offer the detailed stress distribution around the contact surface. A whole-field optical method and a new technique for measuring contact force should be developed for the experimental analysis.

It must be very valuable if some conclusions drawn from relative thin composites can be extended to thick composites. This thesis concludes the importance of the thickness scaling effects in composite joint structures. The investigations on thickness scaling effects in composites should be carried out in many fields.

#### **REFFERENCES**

Harris, D. E. & Morris, D. H., <u>Composite Materials: Testing and Design</u> (7th Conf.)ASTM STP 893.

Bogetti, T. A., Gillespie, J. W. & Pipes, R. B., Report no. 87-55, Center for Composite Materials, University of Delaware.

Workshop on Scaling Effects in Composite Materials and Structures, NASA Langley Research Center, Hampton, VA, November 15-16, 1993, Report No. 94-6, Institute for Mechanics and Materials, University of California, San Diego, CA.

Twardowski, T. E., Lin, S. E. & Geil, P. H., "Curing in Thick Composite Laminates: Experiment and Simulations," Journal of Composite Materials, 27(3), 216-251, 1993.

Alexander, A. & Tzeng, J. T., "Three Dimensional Effective Properties of Composite Materials for Finite Element Applications." Journal of composite Materials, 31(5), 466-476, 1997.

Yang, C., Pang, S. S. & Zhao, Y., "Buckling Analysis of Thick-Walled Composite Pipe under External Pressure," Journal of Composite Materials, 31(4), 409-426, 1997.

Avva, V. S., Allen, H. G. & Shivadumar, D. N., "Through-the-thickness Tension Strength of 3-D Braided Composites," Journal of Composite Materials, 30(1), 51-68, 1996.

Nguyen, B. N., "Three-Dimensional Modeling of Damage in Laminated Composites Containing a Central Hole," Journal of composite Materials, 31(17), 1672-1693, 1997.

Renard, J., Favre, J. P. & Jeggy, T., "Influence of Transverse Cracking on Ply Behavior: Introduction of a Characteristic Damage Variable," Composites Science and Technology, 46(29), 231-267, 1993.

Camponeschi, E. T., Gillespie, J. W., & Wilkins, D. J., "Kink-Band Failure Analysis of Thick Composites in Compression," Journal of Composite Materials, 27(5), 471-491, 1993.

Woo, K. & Whitcomb, J. D., "Three-Dimensional Failure Analysis of Plain Weave Textile composites Using A Global/Local Finite Element Method," Journal of Composite Materials, 30(9), 984-1003, 1996.

Hamada H., Maekawa A., and Haruna R., "Strength Prediction of Mechanically Fastened Quasi-isotropic Carbon/Epoxy Joints," J. Composite Materials, 30(14), 1596-1612, 1996.

- Whitney J. M. and Nuismer R. J., "Stress Fracture Criteria for Laminated Composites Containing Stress Concentrations," J. Composite Materials, 8(2), 253-265, 1974.
- Dattaguru, B. and Rao, A. K. "Contact Problems in Fastener Joints in Composite Plates," Composite Mechanics, 1(20), 542-578, 1988.
- Jong, T. J., <u>Stresses Around a Hole in an Elastically Orthotropic or Isotropic Plate Loaded Through a Pin Which Moves Without Friction in the Hole</u>, Rep. 13, LR-223, Aerospace Dept., Delft University of Technology, 1976.
- Waszcac J. P. and Cruse T. A., <u>A Synthesis Procedure of Mechanically Fastened Joints in Advanced Composite Materials</u>, Dept. of Mech. Engineering, Carnegie-Mellon University, Pittsburgh, Pennsylvania, 1973.
- Jong, T. J., "Stresses Around Pin-Loaded Holes in elastically Orthotropic or Isotropic Plates," Journal of Composite Materials, 11(2), 313-342, 1977.
- Lassard, L. B., Shokrieh, M. M., and Esbensen, J. H., "Analysis of Stress Singularities in Laminated Composite Pinned/Bolted Joints," International SAMPE Symposium, Anaheim, California, 53-60, 1994.
- Hart-Smith L. J., <u>Bolted Joints In Graphite/Eposy Composites</u>, NASA CR-144899, Washington, DC: Nationa Aeronautics and Space Administration, 1978.
- Crews, J.H. and Naik, R. A. "Combined Bearing and Bypass Loading on a Graphite/Eposy Laminate," Composite Structures, 6(6), 21-40, 1986.
- Wang, H. S., Hung, C. L. & Chang, F. K., "Bearing Failure of Bolted Composite Joints. Part 1: Experimental Characterization," Journal of composite Materials, 30(12), 1284-1314, 1996.
- Wang, H. S., Hung, C. L. & Chang, F. K., "Bearing Failure of Bolted Composite Joints. Part 2: Model and Verification," Journal of composite Materials, 30(12), 1359-1399, 1996.
- Sperling, U. O., "Three-Dimensional Stress Distribution Around Pin Loaded Holes in Composite Laminates," AIAA J., 743-750, 1985.
- Sundarrai, N. and Dattaguru, B., "Analysis of a Double Shear Lap Joint with Interference Fit Pin," Computation Structure, 55(2), 357-363, 1995.
- Hwang, D.Y. and Stallings, J. M., "Finite Element Analysis of Bolted Flange Connections", Computation Structure, 51(5), 521-533, 1994.

Griffin, O. H., Hyer, Jr. MD., Cohen, D., Shuart, D. J., Yalamanchili, S. R., and Prasad, C. B., "Analysis of Multifastener Composite Joints," J. Spacecraft Rockets, 31(2), 278-284, 1994.

Ireman T., Nyman T. and Hellbom K., "Design Methods for Bolted Joints in Composite Aircraft Structures," Composite Structure, 25(1-4), 567-578, 1993.

Madenci E. and Ileri L., "Analytical Determination of Contact Stresses in Mechanically Fastened Composite Laminates With Finite Boundaries," International J. Solids Structure, 30(18), 2469-2484, 1993.

Lassard, L. B. and Shokrieh, M. M., "Two-dimensional Modeling of Composite Pinned-Joint Failure," J. Composite Materials, 29(5), 671-697, 1995.

Rajapakse, Y. D. S., <u>Mechanics of Thick Composites</u>, AMD, The American Society of Mechanical Engineers, Vol 162, 1993.

Marshall, I. M., Arnold, W. S., Wood, J., and Mousley, R. F., "Observation on Bolted Connections in Composite Structures," Composite Structures, Vol 13, 133-151, 1989.

Hamada, H., Maekawa, A., and Haruna, K., "Strength Prediction of Mechanically Fastened Quasi-isotropic Carbon/Epoxy Joints," J. Composite Materials, 30(14), 1596-1612, 1996.

Fu-Kuo Chang and Larry B. Lessard, "Damage Tolerance of laminated Composites Containing an Open hole and Subjected to Compressive Loadings," J. Composite Materials, Vol 25, 1991.

		•	
			•
			,

· •			
<b>,</b>			
<b>)</b>			
' }			
<b>)</b> :			
:			
; !			
) 			
<b>1</b>			
<b>₹</b> :			

